LUBAC is essential for embryogenesis by preventing cell death and enabling haematopoiesis

Nieves Peltzer[1]*, Maurice Darding[1]*, Antonella Montinaro[1], Peter Draber[1], Helena Draberova[1], Sebastian Kupka[1], Eva Rieser[1], Amanda Fisher[2], Ciaran Hutchinson[3], Lucia Taraborrelli[1], Torsten Hartwig[1], Elodie Lafont[1], Tobias L. Haas[4], Yutaka Shimizu[1], Charlotta Böiers[1], Aida Sarr[1], James Rickard[5], Silvia Alvarez-Diaz[5], Michael T. Ashworth[3], Allison Beal[6], Tariq Enver[1], John Bertin[6], William Kaiser[2], Andreas Strasser[5], John Silke[5], Philippe Bouillet[5] and Henning Walczak[1,7]

[1]UCL Cancer Institute, University College London, 72 Huntley Street, London WC1E 6DD, UK
[2]University of Texas Health Science Center, 7703 Floyd Curl Drive, San Antonio, TX 78229, USA
[3]UCL Great Ormond Street Institute of Child Health, 30 Guilford St, London, UK
[4]Institute of General Pathology, Università Cattolica del Sacro Cuore, 00168, Rome, Italy
[5]The Walter and Eliza Hall Institute of Medical Research, 1G Royal Parade, Parkville, Victoria 3052, Australia
[6]Pattern Recognition Receptor Discovery Performance Unit, Immuno-Inflammation Therapeutic Area, GlaxoSmithKline, Collegeville, Pennsylvania, USA
[7]Correspondence to: Henning Walczak, PhD; E-mail: h.walczak@ucl.ac.uk. Phone +44 207 679 6471

* These authors contributed equally.

The Linear Ubiquitin chain Assembly Complex (LUBAC) is required for optimal gene activation and prevention of cell death upon activation of immune receptors, including TNFR1[1]. Deficiency in the LUBAC components SHARPIN or HOIP in mice results in severe inflammation in adulthood or embryonic lethality, respectively, due to deregulation of TNFR1-mediated cell death[2-8]. In humans, deficiency in the third LUBAC component, HOIL-1, causes autoimmunity and inflammatory disease, similar to HOIP deficiency, whereas HOIL-1 deficiency in mice was reported to cause no overt phenotype[9-11]. By creating HOIL-1-deficient mice, we here show that HOIL-1 is, however, as essential for LUBAC function as HOIP, albeit for different reasons: whereas HOIP is LUBAC's catalytically active component, HOIL-1 is required for LUBAC assembly, stability and optimal retention in the TNFR1-signalling complex (TNFR1-SC), thereby preventing aberrant cell death. Both, HOIL-1 and HOIP prevent embryonic lethality at mid-gestation by interfering with aberrant TNFR1-mediated endothelial cell death, which only partially depends on RIPK1 kinase activity. Co-deletion of Caspase-8 with RIPK3 or MLKL prevents cell death in *Hoil-1*$^{-/-}$ embryos, yet only combined loss of Caspase-8 with MLKL results in viable HOIL-1-deficient mice. Interestingly, *Ripk3*$^{-/-}$*Caspase-8*$^{-/-}$ *Hoil-1*$^{-/-}$ embryos die at late-gestation due to haematopoietic defects that are rescued by co-deletion of RIPK1 but not MLKL. Collectively, these results demonstrate that both, HOIP and HOIL-1 are essential LUBAC components and are required for embryogenesis by preventing aberrant cell death. Furthermore, they unveil that, when LUBAC and Caspase-8 are absent, RIPK3 prevents RIPK1 from inducing embryonic lethality by causing defects in foetal haematopoiesis.

To determine the physiological role of HOIL-1, we generated HOIL-1-deficient mice by targeting exons 1 and 2 of the *Hoil-1 (Rbck1)* gene (**Extended Data Fig. 1a-d**). No mice with homozygous deletion in the *Hoil-1* gene were weaned (**Fig. 1a**). Analysis of *Hoil-1*$^{-/-}$ embryos revealed that they died around embryonic day (E) 10.5 (**Fig. 1a, b**). This result was confirmed with a strain generated from an independently targeted ES cell (C20*Hoil-1*$^{-/-}$ mice) (**Extended Data Fig. 1e, f**). At E10.5, *Hoil-1*$^{-/-}$ embryos presented with disrupted vascular architecture and cell death in the yolk sac endothelium (**Fig. 1c, d** and **Extended Data Fig. 1g, h**), indicating that HOIL-1 absence causes aberrant endothelial cell death. *Hoil-1*$^{fl/fl}$*Tie2-Cre+* (endothelium/some haematopoietic cell-specific cre) embryos also died around E10.5 with the same abnormalities (**Fig. 1e** and **Extended Data Fig. 1i, j**). Loss of TNF or TNFR1 diminished cell death in the yolk sac and prevented lethality at E10.5 in *Hoil-1*$^{-/-}$ embryos (**Fig. 1f** and **Extended Data Fig. 2a-d**). As in *Tnfr1*$^{-/-}$*Hoip*$^{-/-}$[8], *Tnfr1*$^{-/-}$*Hoil-1*$^{-/-}$ yolk sacs showed reduced cell death as compared to *Hoil-1*$^{-/-}$ embryos (**Fig. 1f, g**). Although cell death was not completely ablated in *Tnfr1*$^{-/-}$*Hoil-1*$^{-/-}$ embryos, it did not appear to significantly affect yolk sac vasculature (**Fig. 1f, g** and **Extended Data Fig. 2e**). Nevertheless, *Tnfr1*$^{-/-}$*Hoil-1*$^{-/-}$ embryos died around E16.5 (**Extended Data Fig. 2d, f**) with heart defects prior to death (**Fig. 1h**). Therefore, like HOIP, HOIL-1 is required to maintain blood vessel integrity by preventing TNFR1-mediated endothelial cell death during embryogenesis.

To understand the role of HOIL-1 in LUBAC function, we compared TNFR1-SC formation in MEFs individually deficient for the LUBAC components. Whereas in SHARPIN-deficient MEFs TNFR1-SC-associated linear ubiquitination was merely reduced[7], it was completely absent in *Tnf*$^{-/-}$*Hoil-1*$^{-/-}$ MEFs, exactly as in *Tnf*$^{-/-}$*Hoip*$^{-/-}$ MEFs[8] (**Fig. 2a**). In TNF-stimulated *Tnf*$^{-/-}$*Hoil-1*$^{-/-}$ MEFs, NF-κB activation was attenuated (**Extended Data Fig. 3a**) and TNFR1 complex-II formation was enhanced (**Fig. 2b**), resulting in sensitisation to TNF-induced apoptosis and necroptosis (**Fig. 2c**). Hence, HOIL-1 is as essential as HOIP for linear ubiquitination within the TNFR1-SC.

To determine whether the reduction in HOIP and SHARPIN protein levels in HOIL-1-deficient cells was responsible for the observed loss of linear ubiquitination (**Fig. 2a**), we reconstituted HOIL-1-deficient MEFs with HOIP, with HOIP and SHARPIN, or, as a control, with HOIL-1. Reconstitution with HOIP, either alone or with SHARPIN, failed to restore LUBAC recruitment, linear ubiquitination at the TNFR1-SC, or optimal NF-κB activation. Furthermore, their reconstitution was unable to prevent TNF-induced complex-II formation and cell death (**Fig. 2d-f** and **Extended Data Fig. 3b**) whilst HOIL-1 re-expression corrected all aforementioned defects (**Fig. 2d-f** and **Extended Data Fig. 3b**). In the absence of HOIL-1, HOIP was unable to bind to SHARPIN despite both being reconstituted to near endogenous levels (**Extended Data Fig. 3c**). Thus, HOIL-1 is required for LUBAC assembly and recruitment to the TNFR1-SC, identifying it as an essential component of LUBAC alongside HOIP.

To reveal how HOIL-1 enables LUBAC activity, we generated HOIL-1-deficient MEFs stably expressing full-length HOIL-1 (WT), the UBL domain of HOIL-1 only (HOIL-1-UBL), HOIL-1-ΔRBR, HOIL-1-ΔUBL, HOIL-1 with inactivating mutations T201A/R208A in the NZF domain (HOIL-1-NZFmut) or HOIL-1 with a point mutation in the catalytic cysteine of the RBR domain (HOIL-1-C458A) (**Fig. 2g**). Except for HOIL-1-ΔUBL, all mutant HOIL-1 proteins bound to HOIP and SHARPIN and stabilised their levels (**Fig. 2h**). Isolation of the native TNFR1-SC revealed that HOIL-1-ΔRBR and HOIL-1-C458A fully restored TNF-induced linear ubiquitination in HOIL-1-deficient cells, whereas HOIL-1-ΔUBL did not (**Fig. 2i**). HOIL-1-deficient cells expressing HOIL-1-UBL or HOIL-1-NZFmut only showed partial restoration of linear ubiquitination, correlating with reduced HOIP and SHARPIN levels at the TNFR1-SC (**Fig. 2i**). Thus, the UBL domain of HOIL-1 is essential for linear ubiquitination at the TNFR1-SC, whereas a functional NZF domain is required for optimal LUBAC presence in the TNFR1-SC. Expression of HOIL-1-ΔRBR restored optimal NF-κB signalling and prevented aberrant TNF-induced cell killing in contrast to HOIL-1-ΔUBL (**Fig. 2j** and **Extended Data Fig. 3d**). This observation elucidates why the previously reported mice, regarded as deficient for HOIL-1, are viable as they were generated by targeting exons 7 and 8[12], likely resembling the HOIL-1-ΔRBR mutant studied here. Since the UBL of HOIL-1 binds to HOIP, allowing its activation[13] and the NZF of HOIL-1 binds linear ubiquitin linkages[14], our results provide evidence that HOIL-1 promotes HOIP activation as well as LUBAC assembly and recruitment to the TNFR1-SC via its UBL domain. Once linear ubiquitin chains are formed in the complex, the NZF domain of HOIL-1 promotes LUBAC retention by binding to these chains.

Since both HOIL-1 and HOIP are equally important for LUBAC function and, consequently, for preventing aberrant cell death *in vitro* and *in vivo*, we used a genetic strategy to untangle the interplay between HOIL-1 or HOIP and the different cell death components. Inactivation of RIPK1 in *Hoil-1*$^{-/-}$ and *Hoip*$^{-/-}$ embryos delayed lethality until E14.5 (**Fig. 3a** and **Extended Data Fig. 4a-d**). At this time, *Ripk1*^{K45A}*Hoil-1*$^{-/-}$ and *Ripk1*^{K45A}*Hoip*$^{-/-}$ embryos had disrupted vascular architecture, excessive cell death in their yolk sacs, hearts, livers and lungs and presented with heart defects and liver necrosis (**Fig. 3b** and **Extended Data Fig. 4e-h**). In accordance, TNFR1 complex-II formation and aberrant TNF/LT-α-induced apoptosis were only partially inhibited in *Ripk1*^{K45A}*Hoil-1*$^{-/-}$ MEFs (**Fig. 3c, d and Extended Data Fig. 4i**). Thus, whilst the kinase activity of RIPK1 is essential for excessive TNFR1-induced cell death caused by attenuated LUBAC activity, as previously observed in SHARPIN-deficient mice[4], this is not the case when LUBAC activity is completely abrogated.

We next tested whether loss of RIPK3, MLKL or Caspase-8 could prevent lethality in *Hoip*$^{-/-}$ and *Hoil-1*$^{-/-}$ embryos. At E10.5, *Ripk3*$^{-/-}$*Hoil-1*$^{-/-}$ embryos presented with defects in vascularisation, excessive cell death and died at mid-gestation **(Extended Data Fig. 5b, c**). Due to the close

chromosomal linkage of HOIP and RIPK3, we generated *Mlkl*$^{-/-}$*Hoip*$^{-/-}$ mice (**Extended Data Fig. 5a**). These embryos also died at mid-gestation (**Extended Data Fig. 5d**). Likewise, neither Caspase-8 heterozygosity nor Caspase-8 full deletion was sufficient to prevent the mid-gestation lethality of *Hoip*$^{-/-}$ and *Hoil-1*$^{-/-}$ embryos (**Extended Data Fig. 5e, f** and data not shown).

As RIPK3-mediated necroptosis may be responsible for the embryonic lethality of *Caspase-8*$^{+/-}$*Hoil-1*$^{-/-}$ or *Caspase-8*$^{-/-}$*Hoil-1*$^{-/-}$ mice[15,16], we generated *Ripk3*$^{-/-}$*Caspase-8*$^{+/-}$*Hoil-1*$^{-/-}$ and *Ripk3*$^{-/-}$*Caspase-8*$^{-/-}$*Hoil-1*$^{-/-}$ embryos and in both cases the lethality was delayed until around E14.5 (**Fig. 3e** and **Extended Data Fig. 6a, b**). At this developmental stage, a single intact copy of Caspase-8 was sufficient to induce apoptosis-driven loss of yolk sac vascularisation (**Fig. 3f** and **Extended Data Fig. 6c, d**). Yet, although *Ripk3*$^{-/-}$*Caspase-8*$^{-/-}$*Hoil-1*$^{-/-}$ embryos died around E14.5, yolk sac vascularisation was normalised and cell death in the yolk sac and other organs was prevented (**Fig. 3f** and **Extended Data Fig. 6c-f**). Moreover, *Ripk3*$^{-/-}$*Caspase-8*$^{-/-}$*Hoil-1*$^{-/-}$ MEFs were resistant to cell death induced by TNF or related cytokines (**Extended Data Fig. 6g**). Histological examination and microfocus CT scanning revealed the presence of heart defects in both *Ripk3*$^{-/-}$*Caspase-8*$^{-/-}$*Hoil-1*$^{-/-}$ and *Ripk3*$^{-/-}$*Caspase-8*$^{+/-}$*Hoil-1*$^{-/-}$ embryos (**Extended Data Fig. 6h, i**). We therefore conclude that whereas mid-gestation lethality in *Hoil-1*$^{-/-}$ embryos is dependent on Caspase-8/RIPK3-dependent apoptosis and necroptosis, *Ripk3*$^{-/-}$*Caspase-8*$^{-/-}$*Hoil-1*$^{-/-}$ embryos die at late gestation by a process that is independent of cell death.

In striking contrast to *Ripk3*$^{-/-}$*Caspase-8*$^{-/-}$*Hoil-1*$^{-/-}$ mice, both *Mlkl*$^{-/-}$*Caspase-8*$^{-/-}$*Hoil-1*$^{-/-}$ and *Mlkl*$^{-/-}$*Caspase-8*$^{-/-}$*Hoip*$^{-/-}$ mice were born, albeit at lower than expected Mendelian ratios (**Fig. 3g** and **Extended Data Fig. 7a**). These mice were runted and had to be sacrificed by 4-5 weeks of age. Histopathological analysis revealed severe inflammation in the liver and lungs (**Fig. 3h, Extended Data Fig. 7b-d** and data not shown). Of note, *Caspase-8* heterozygosity resulted in increased apoptosis of endothelial cells, causing lethality in both *Mlkl*$^{-/-}$*Caspase-8*$^{+/-}$*Hoip*$^{-/-}$ and *Mlkl*$^{-/-}$*Caspase-8*$^{+/-}$*Hoil-1*$^{-/-}$ embryos around E14.5 (**Extended Data Fig. 7e** and data not shown) indicating that Caspase-8-driven apoptosis is sufficient to cause death of LUBAC-deficient embryos.

Co-deletion of RIPK3 and Caspase-8 causes embryonic lethality in otherwise viable *cpdm* mice[7]. However, *Mlkl*$^{-/-}$*Caspase-8*$^{-/-}$*cpdm* mice were viable and the inflammatory syndrome that characterises *cpdm* mice was prevented (**Fig. 3i and Extended Data Fig. 7f, g**), whilst expectedly[17] developing lymphadenopathy and splenomegaly (**Fig. 3i and Extended Data Fig. 7f)**. Thus, combined loss of any of the three LUBAC components together with loss of Caspase-8 uncovers a vital functional difference between RIPK3 and MLKL.

We next evaluated whether the lethality of *Ripk3*$^{-/-}$*Caspase-8*$^{-/-}$*Hoil-1*$^{-/-}$ mice is due to aberrant (RIPK3-independent) MLKL activation. This was particularly pertinent because MLKL levels were increased in *Ripk3*$^{-/-}$*Caspase-8*$^{-/-}$*Hoil-1*$^{-/-}$ embryos and MLKL was aberrantly activated in some of them (**Extended Data Fig. 7h**). However, MLKL co-deficiency did not prevent the death of *Ripk3*$^{-/-}$ *Caspase-8*$^{-/-}$*Hoil-1*$^{-/-}$ embryos (**Fig. 3j** and **Extended Data Fig. 7h**). Thus, RIPK3 is required for survival of embryos in the absence of LUBAC by regulating an MLKL-independent process.

To explore the nature of the pro-survival role of RIPK3, we performed RNAseq on E13.5 *Ripk3*$^{-/-}$ *Caspase-8*$^{-/-}$*Hoil-1*$^{-/-}$ and *Mlkl*$^{-/-}$*Caspase-8*$^{-/-}$*Hoil-1*$^{-/-}$ embryos and controls (**Extended Data Fig. 8a** and **Supplementary Table 1**). Gene Ontology (GO) enrichment analysis of differentially expressed genes pointed towards defects in erythropoiesis in *Ripk3*$^{-/-}$*Caspase-8*$^{-/-}$*Hoil-1*$^{-/-}$ embryos (**Extended Data Fig. 8b**). Indeed, reduced levels of erythroid lineage Ter119^{+} cells (**Fig. 4a**), basophilic erythroblasts (**Extended Data Fig. 8c**) and mature erythrocytes (**Fig. 4b**) were observed in of *Ripk3*$^{-/-}$*Caspase-8*$^{-/-}$ *Hoil-1*$^{-/-}$ foetal livers. Furthermore, *Ripk3*$^{-/-}$*Caspase-8*$^{-/-}$*Hoil-1*$^{-/-}$ haematopoietic progenitors failed to differentiate into committed erythroid burst-forming units in culture (**Fig. 4e**). Further analysis of the haematopoietic compartment from E13.5 foetal livers revealed abnormally reduced percentages and total numbers of multipotent progenitors (**Fig. 4d** and **Extended Data Fig. 8d, e**) as well as leucocytes, including granulocytes and macrophages, and myeloid progenitors in the *Ripk3*$^{-/-}$*Caspase-8*$^{-/-}$*Hoil-1*$^{-/-}$ embryos compared to controls, whereas *Mlkl*$^{-/-}$*Caspase-8*$^{-/-}$*Hoil-1*$^{-/-}$ embryos had normal numbers of these cells (**Extended Data Fig. 8f-k**). In addition, the capacity of haematopoietic progenitors to generate colony-forming myeloid progenitors and multi-potent progenitors was also impaired in the *Ripk3*$^{-/-}$*Caspase-8*$^{-/-}$*Hoil-1*$^{-/-}$ embryos (**Extended Data Fig. 8l**). Accordingly, the viability of macrophages obtained from *Ripk3*$^{-/-}$*Caspase-8*$^{-/-}$*Hoil-1*$^{-/-}$ foetal liver cell suspensions in culture was significantly lower than those of controls and this could not be rescued by inhibiting necroptosis or apoptosis. *Mlkl*$^{-/-}$*Caspase-8*$^{-/-}$*Hoil-1*$^{-/-}$ foetal liver cells, however, produced normal numbers of macrophages (**Extended Data Fig. 4m**). Despite the heart defects of *Ripk3*$^{-/-}$*Caspase-8*$^{-/-}$ *Hoil-1*$^{-/-}$ embryos, blood circulation was normal at E13.5 and the percentages of CD45^{+}cKIT^{+} cells obtained from aorta-gonad-mesonephros regions were comparable between *Ripk3*$^{-/-}$*Caspase-8*$^{-/-}$*Hoil-1*$^{-/-}$ embryos and controls at E11.5 (Extended Data **Fig. 8o, p**). We therefore conclude that *Ripk3*$^{-/-}$ *Caspase-8*$^{-/-}$*Hoil-1*$^{-/-}$ embryos suffer from intrinsic defects in early haematopoiesis, likely downstream of specification in the aorta-gonad-mesonephros, resulting in substantial deficiencies in erythroid and myeloid cells.

Since LUBAC is known to regulate RIPK1[24], we investigated the role of RIPK1 in the lethality of *Ripk3*$^{-/-}$*Caspase-8*$^{-/-}$*Hoil-1*$^{-/-}$ embryos. Lethality of *Ripk3*$^{-/-}$*Caspase-8*$^{-/-}$*Hoil-1*$^{-/-}$ embryos was prevented by additional loss of RIPK1, despite RIPK1 levels being relatively low in *Ripk3*$^{-/-}$*Caspase-8*$^{-/-}$*Hoil-1*$^{-/-}$ embryos and RIPK1 deficiency failing to prevent *Hoil-1*$^{-/-}$ embryonic lethality (**Fig. 4d, e and**

Extended Data Fig. 7h and 9a, b). Importantly, the viability of macrophages obtained from *Ripk1*$^{-/-}$ *Ripk3*$^{-/-}$*Caspase-8*$^{-/-}$*Hoil-1*$^{-/-}$ foetal livers was comparable to controls (**Extended Data Fig. 9c**), indicating normalised haematopoiesis in these mice. The expression of several cytokines, including IL-1β, CCL2, IFN-β and CXCL10, was abnormally increased in *Ripk3*$^{-/-}$*Caspase-8*$^{-/-}$*Hoil-1*$^{-/-}$ embryos but not in *Ripk1*$^{-/-}$*Ripk3*$^{-/-}$*Caspase-8*$^{-/-}$*Hoil-1*$^{-/-}$ embryos **(Fig. 4f and Extended Data Fig. 9d, e)**. The function, survival, differentiation and self-renewal of haematopoietic progenitors are greatly impacted by various of these cytokines[18,19]. Therefore, our findings suggest that RIPK1-driven deregulated cytokine production in *Ripk3*$^{-/-}$*Caspase-8*$^{-/-}$*Hoil-1*$^{-/-}$ embryos may impair foetal haematopoiesis. Finally, treatment of pregnant females with the RIPK1 kinase inhibitor GSK'547A[20] did not prevent lethality of *Ripk3*$^{-/-}$*Caspase-8*$^{-/-}$*Hoil-1*$^{-/-}$ embryos, although it was able to extend the survival of *Ripk3*$^{-/-}$ *Caspase-8*$^{+/-}$*Hoil-1*$^{-/-}$ embryos (**Extended Data Fig. 9f**). These results suggest that the lethality of *Ripk3*$^{-/-}$*Caspase-8*$^{-/-}$*Hoil-1*$^{-/-}$ embryos likely depends on the scaffolding function of RIPK1.

Although RIPK1 is required for emergency haematopoiesis, RIPK1 might regulate embryonic haematopoiesis differently. Indeed, RIPK1-constitutive or haematopoietic-cell-specific-deficient mice are not embryonically lethal[21,22]. In addition, absence of LUBAC, RIPK3 and Caspase-8 might affect mechanisms during embryogenesis that are different from those perturbed by RIPK1 deficiency alone. Collectively, our findings imply that in the combined absence of LUBAC and Caspase-8, RIPK3 exerts a pro-survival role by regulating RIPK1-mediated signalling (**Extended Data Fig. 10**). Since *Ripk3*$^{-/-}$*Caspase-8*$^{-/-}$ mice are viable[15,16,23], our findings indicate that control of RIPK1 by either LUBAC or RIPK3 is sufficient to enable proper haematopoiesis in the developing embryo, likely by preventing deregulated cytokine production. Thus, LUBAC and RIPK3 control RIPK1-mediated signalling to allow embryonic haematopoiesis.

REFERENCES

1 Shimizu, Y., Taraborrelli, L. & Walczak, H. Linear ubiquitination in immunity. *Immunological reviews* **266**, 190-207, doi:10.1111/imr.12309 (2015).

2 Sasaki, Y. *et al.* Defective immune responses in mice lacking LUBAC-mediated linear ubiquitination in B cells. *EMBO J* **32**, 2463-2476, doi:10.1038/emboj.2013.184 (2013).

3 Emmerich, C. H. *et al.* Activation of the canonical IKK complex by K63/M1-linked hybrid ubiquitin chains. *Proc Natl Acad Sci U S A* **110**, 15247-15252, doi:10.1073/pnas.1314715110 (2013).

4 Berger, S. B. *et al.* Cutting Edge: RIP1 kinase activity is dispensable for normal development but is a key regulator of inflammation in SHARPIN-deficient mice. *J Immunol* **192**, 5476-5480, doi:10.4049/jimmunol.1400499 (2014).

5 Gerlach, B. *et al.* Linear ubiquitination prevents inflammation and regulates immune signalling. *Nature* **471**, 591-596, doi:10.1038/nature09816 (2011).

6 Kumari, S. *et al.* Sharpin prevents skin inflammation by inhibiting TNFR1-induced keratinocyte apoptosis. *eLife* **3**, doi:10.7554/eLife.03422 (2014).

7 Rickard, J. A. *et al.* TNFR1-dependent cell death drives inflammation in Sharpin-deficient mice. *eLife* **3**, doi:10.7554/eLife.03464 (2014).

8 Peltzer, N. *et al.* HOIP deficiency causes embryonic lethality by aberrant TNFR1-mediated endothelial cell death. *Cell Rep* **9**, 153-165, doi:10.1016/j.celrep.2014.08.066 (2014).

9 Boisson, B. *et al.* Immunodeficiency, autoinflammation and amylopectinosis in humans with inherited HOIL-1 and LUBAC deficiency. *Nat Immunol* **13**, 1178-1186, doi:10.1038/ni.2457 (2012).

10 Boisson, B. *et al.* Human HOIP and LUBAC deficiency underlies autoinflammation, immunodeficiency, amylopectinosis, and lymphangiectasia. *J Exp Med* **212**, 939-951, doi:10.1084/jem.20141130 (2015).

11 Tokunaga, F. *et al.* Involvement of linear polyubiquitylation of NEMO in NF-kappaB activation. *Nat Cell Biol*, doi:10.1038/ncb1821 (2009).

12 Tokunaga, F. *et al.* Involvement of linear polyubiquitylation of NEMO in NF-kappaB activation. *Nat Cell Biol* **11**, 123-132, doi:10.1038/ncb1821 (2009).

13 Stieglitz, B., Morris-Davies, A. C., Koliopoulos, M. G., Christodoulou, E. & Rittinger, K. LUBAC synthesizes linear ubiquitin chains via a thioester intermediate. *EMBO Rep* **13**, 840-846, doi:10.1038/embor.2012.105 (2012).

14 Sato, Y. *et al.* Specific recognition of linear ubiquitin chains by the Npl4 zinc finger (NZF) domain of the HOIL-1L subunit of the linear ubiquitin chain assembly complex. *Proc Natl Acad Sci U S A* **108**, 20520-20525, doi:10.1073/pnas.1109088108 (2011).

15 Kaiser, W. J. *et al.* RIP3 mediates the embryonic lethality of caspase-8-deficient mice. *Nature* **471**, 368-372, doi:10.1038/nature09857 (2011).

16 Oberst, A. *et al.* Catalytic activity of the caspase-8-FLIP(L) complex inhibits RIPK3-dependent necrosis. *Nature* **471**, 363-367, doi:10.1038/nature09852 (2011).

17 Alvarez-Diaz, S. *et al.* The Pseudokinase MLKL and the Kinase RIPK3 Have Distinct Roles in Autoimmune Disease Caused by Loss of Death-Receptor-Induced Apoptosis. *Immunity*, doi:10.1016/j.immuni.2016.07.016 (2016).

18 Clapes, T., Lefkopoulos, S. & Trompouki, E. Stress and Non-Stress Roles of Inflammatory Signals during HSC Emergence and Maintenance. *Front Immunol* **7**, 487, doi:10.3389/fimmu.2016.00487 (2016).

19 Pietras, E. M. Inflammation: a key regulator of hematopoietic stem cell fate in health and disease. *Blood* **130**, 1693-1698, doi:10.1182/blood-2017-06-780882 (2017).

20 Harris, P. A. *et al.* Discovery of a First-in-Class Receptor Interacting Protein 1 (RIP1) Kinase Specific Clinical Candidate (GSK2982772) for the Treatment of Inflammatory Diseases. *Journal of Medicinal Chemistry* **60**, 1247-1261, doi:10.1021/acs.jmedchem.6b01751 (2017).

21 Roderick, J. E. *et al.* Hematopoietic RIPK1 deficiency results in bone marrow failure caused by apoptosis and RIPK3-mediated necroptosis. *Proc Natl Acad Sci U S A* **111**, 14436-14441, doi:10.1073/pnas.1409389111 (2014).
22 Rickard, J. A. *et al.* RIPK1 regulates RIPK3-MLKL-driven systemic inflammation and emergency hematopoiesis. *Cell* **157**, 1175-1188, doi:10.1016/j.cell.2014.04.019 (2014).
23 Dillon, C. P. *et al.* Survival function of the FADD-CASPASE-8-cFLIP(L) complex. *Cell Rep* **1**, 401-407, doi:10.1016/j.celrep.2012.03.010 (2012).
24 Peltzer, N., Darding, M. & Walczak, H. Holding RIPK1 on the Ubiquitin Leash in TNFR1 Signaling. *Trends Cell Biol* **26**, 445-461, doi:10.1016/j.tcb.2016.01.006 (2016).
25 Gustafsson, E., Brakebusch, C., Hietanen, K. & Fassler, R. Tie-1-directed expression of Cre recombinase in endothelial cells of embryoid bodies and transgenic mice. *Journal of cell science* **114**, 671-676 (2001).
26 Murphy, J. M. *et al.* The pseudokinase MLKL mediates necroptosis via a molecular switch mechanism. *Immunity* **39**, 443-453, doi:10.1016/j.immuni.2013.06.018 (2013).
27 Newton, K., Sun, X. & Dixit, V. M. Kinase RIP3 is dispensable for normal NF-kappa Bs, signaling by the B-cell and T-cell receptors, tumor necrosis factor receptor 1, and Toll-like receptors 2 and 4. *Molecular and cellular biology* **24**, 1464-1469 (2004).
28 Salmena, L. *et al.* Essential role for caspase 8 in T-cell homeostasis and T-cell-mediated immunity. *Genes & development* **17**, 883-895, doi:10.1101/gad.1063703 (2003).
29 Kelliher, M. A. *et al.* The death domain kinase RIP mediates the TNF-induced NF-kappaB signal. *Immunity* **8**, 297-303 (1998).
30 Haas, T. L. *et al.* Recruitment of the linear ubiquitin chain assembly complex stabilizes the TNF-R1 signaling complex and is required for TNF-mediated gene induction. *Mol Cell* **36**, 831-844, doi:10.1016/j.molcel.2009.10.013 (2009).

Acknowledgements

Drs Vishva Dixit and Kim Newton (Genentech) provided *Ripk3*$^{-/-}$ mice, Drs Stephen Hedrick and Razq Hakem (University of Toronto) provided *Caspase-8*$^{fl/fl}$ mice; Holly Anderton and Dr Ueli Nachbur at (WEHI) helped with *cpdm* analysis; Paul Levy and staff (UCL) and Lorraine Lawrence at the NHLI (Imperial College) provided technical and histology services. Ashley Leister and Jill Marinis (GSK) advised on GSK'457A. Dr Teresa Marafioti and Ayse Akarsa (UCL) helped with p-MLKL detection. Alessandro Annibaldi (ICR, London, UK) provided helpful discussions and technical assistance. The Microscopy and Imaging Core Facility Facility is supported by the Cancer Research UK (UCL-Centre). This work was funded by a Wellcome Trust Senior Investigator Award (096831/Z/11/Z) and an ERC Advanced grant (294880) awarded to H.W., NHMRC grants awarded to P.B., A.S., J.S. and H.W. (602516, 1037321, 1043414, 1080321, 1105209, 461221, 1042629, 1057905), the Leukemia and Lymphoma Society (Specialised Center of Research grant 7015) and a postdoctoral fellowship awarded to N.P. by the Swiss National Science Foundation (P300P3_158509).

Author Contributions

H.W. conceived the project. N.P. and M.D. performed the majority of the experiments. N.P., M.D. and H.W. designed the research and co-wrote the manuscript. A.M., C.B. and T.E. conceived and

contributed to the haematopoietic analyses. H.D. and P.D. contributed to *in vitro* experiments in Figure 2 and Extended Data Fig. 3, S.K. generated *Mlkl*$^{-/-}$ mice, L.T., E.R. contributed to *in vivo* experiments, T.H performed cytokine arrays and E.L. and Y.S. contributed with biochemistry data. P.B., T.L.H. and H.W. designed the *Hoil-1* floxed allele and P.B. generated it. A.F. and W.K. generated and analysed *Ripk1*$^{-/-}$*Ripk3*$^{-/-}$*Caspase-8*$^{-/-}$*Hoil-1*$^{-/-}$ mice. H.D. and A.S. performed genotyping. A.B. and J.B. provided GSK'547A and *Ripk1*^{K45A} mice. J.R., S.A.D., A.St. and J.S. performed the *cdpm* studies. C.H. and M.T.A. performed pathological and microCT analyses. T.E., P.B., A.St., J.S. and E.R. provided scientific insight.

Author Information

Reprints and permissions information is available at www.nature.com/reprints. The authors declare no competing financial interest. J.B and A.L. are GSK employees. Correspondence and requests for materials should be addressed to h.walczak@ucl.ac.uk.

Figure Legends

Figure 1: HOIL-1 deficiency causes embryonic lethality at mid-gestation due to TNFR1-mediated endothelial cell death

a, Mendelian frequencies obtained from inter-crossing *Hoil-1*$^{+/-}$ mice, *: dead embryos. **b,** Representative images of embryos from E9.5 to E11.5 quantified in (a), *: poor yolk sac vascularisation. Scale bar: 2 mm. **c,** Representative images of yolk sac vascularisation (PECAM-1, red) and cell death (cleaved (cl.) Caspase-3 staining, green) at E10.5 (top panel) (*n*=4 yolk-sacs/genotype), and whole-mount TUNEL staining (bottom, panel) (*n*=2 yolk-sacs/genotype). Scale bar: 50 µm. **d, g,** Quantification of branching points (g) and cleaved Caspase-3 positive cells (g). Mean ± s.e.m. values and *P* values from unpaired two-tailed *t*-tests are shown. **e,** Representative images of embryos at E10.5 (*n*=14 *Hoil-1*$^{fl/wt}$*Tie2-Cre*+ and *n*=7 *Hoil-1*$^{fl/fl}$*Tie2-Cre*+ embryos, top panel). *: poor yolk sac vascularisation. Scale bar: 2 mm. Yolk sac vascularisation (PECAM-1, red) and apoptosis (cleaved Caspase-3, green) (middle panel). Scale bar: 50 µm. Yolk sac whole-mount TUNEL staining (*n*=6 *Hoil-1*$^{fl/wt}$*Tie2-Cre*+ and *n*=2 *Hoil-1*$^{fl/fl}$*Tie2-Cre*+ yolk-sacs/genotype, bottom panel). **f**, Representative images of embryos at E15.5 (top panel, *n*=6 *Tnfr1*$^{-/-}$*Hoil-1*$^{-/-}$ and *n*=19 *Tnfr1*$^{-/-}$ *Hoil-1*$^{+/-}$ embryos), scale bar: 2 mm, and yolk sac vascularisation (PECAM-1, red) and apoptosis (cleaved Caspase-3, green) (bottom panel), Scale bar: 50 µm. **h,** Representative images of H&E staining on whole-embryo paraffin sections (*n*=3 embryos/genotype). *: pericardial effusion, arrows; congested vessels. H, heart; L, lung; Li, liver. Scale bar: 50 µm.

Figure 2: The UBL domain but not the RBR domain of HOIL-1 is essential for LUBAC activity at the TNFR1-SC and to prevent TNF/TNFR1-induced cell death.

a, d, TNFR1-SC pull-down by FLAG- immunoprecipitation (IP) in MEFs derived from mice of the indicated genotypes ± FLAG-TNF for 15 min (*n*=2 independent experiments) (a) and reconstituted with HOIL-1, HOIP or HOIP and SHARPIN (*n*=4 independent experiments) (d). **b, e,** FADD-IP performed in MEFs of the indicated genotypes treated for 4 h with the caspase inhibitor zVAD-fmk ± TNF (b) and reconstituted as indicated (e) (*n*=2 independent experiments (b,e)). **c, f, j,** Cell death analysed by propidium iodide (PI) staining in MEFs with the indicated genotypes ± TNF ± the indicated inhibitors for 24 h (c), reconstituted (f) or transduced (j) as indicated (f, j). Mean ± s.e.m. (*n*=3 independent experiments) and *P* values from two-way ANOVA are shown. **g,** Schematic overview of HOIL-1 constructs used to transduce *Tnf*$^{-/-}$*Hoil-1*$^{-/-}$ MEFs. **h,** Flag-IP of indicated HOIL-1 mutants (*n*=2 independent experiments). **i,** Endogenous TNFR1-SC pull-down by HA-IP in reconstituted *Tnf*$^{-/-}$*Hoil-1*$^{-/-}$ MEFs ± HA-TNF for 15 min (*n*=2 independent experiments). TL: total lysate, NT: not treated, EV: empty vector. For gel source data (a,b,d,e,h,i), see Supplementary Figure 1.

Figure 3: Concomitant loss of MLKL and Caspase-8, but not loss of RIPK1 kinase activity or combined loss of RIPK3 and Caspase-8, promotes survival of LUBAC-deficient mice

a, Representative images of E10.5 (*n*=6 embryos/genotype), scale bar: 2 mm, E14.5 (*n*=12 *Ripk1*^{K45A}*Hoil-1*$^{+/-}$, *n*=5 *Ripk1*^{K45A}*Hoil-1*$^{-/-}$ embryos/genotype) and E15.5 embryos (*n*=3 embryos/genotype). Scale bar: 5 mm. *: poor yolk sac vascularisation. **b, f,** Representative images of yolk sac vascularisation (PECAM-1, red) and apoptosis (cleaved (cl.) Caspase-3, green) at E14.5 (b) or E13.5 (f) and quantification. Mean ± s.e.m. and *P* values from unpaired two-tailed *t*-tests (b) or one-way ANOVA (f) are shown. Scale bar: 50 µm. **c,** FADD-IP in MEFs treated for 3 h with zVAD-fmk ± TNF (*n*=2 independent experiments). For gel source data, see Supplementary Figure 1. **d,** Cell death by PI incorporation in MEFs ± TNF (10 ng/ml) or LT-α. Mean ± s.e.m. (*n*=3 independent experiments) and *P* values (****P<0.0001) from two-way ANOVA are reported. NT: not treated. **e,** Representative images of E14.5 (*n*=11 *Ripk3*$^{-/-}$*Caspase-8*$^{-/-}$*Hoil-1*$^{+/-}$, *Ripk3*$^{-/-}$*Caspase-8*$^{+/-}$*Hoil-1*$^{-/-}$ and *n*=7 *Ripk3*$^{-/-}$*Caspase-8*$^{-/-}$*Hoil-1*$^{-/-}$) and E15.5 embryos (*n*=5 *Ripk3*$^{-/-}$*Caspase-8*$^{-/-}$*Hoil-1*$^{+/-}$, *n*=4 *Ripk3*$^{-/-}$*Caspase-8*$^{+/-}$*Hoil-1*$^{-/-}$ and *n*=8 *Ripk3*$^{-/-}$*Caspase-8*$^{-/-}$*Hoil-1*$^{-/-}$). *: poor yolk sac vascularisation. Scale bar: 5 mm. **g, j,** Mendelian frequencies obtained from inter-crossing *Mlkl*$^{-/-}$*Caspase-8*$^{+/-}$*Hoil-1*$^{+/-}$ with *Mlkl*$^{-/-}$*Caspase-8*$^{-/-}$*Hoil-1*$^{+/-}$ mice (g) or *Mlkl*$^{+/-}$*Ripk3*$^{-/-}$*Caspase-8*$^{-/-}$*Hoil-1*$^{+/-}$ with *Mlkl*$^{-/-}$*Ripk3*$^{-/-}$*Caspase-8*$^{-/-}$*Hoil-1*$^{+/-}$ mice (top) or *Mlkl*$^{-/-}$*Ripk3*$^{-/-}$*Caspase-8*$^{-/-}$*Hoil-1*$^{+/-}$ mice (bottom) (j). *: dead embryos. **h, i,** Representative images of adult mice quantified in (g) for (h) or *n*=3 mice/genotype in (i). m: *cpdm* mutation.

Figure 4: Combined deletion of RIPK3 and Caspase-8 causes haematopoietic defects and RIPK1-dependent embryonic lethality in HOIL-1-deficient mice.

a, b, Number (No.) of the TER119^{+} (erythroid) cells (a) and enucleated erythrocytes/high-power field (HPF) (b) in E13.5 foetal livers with the indicated genotypes. Mean ± s.e.m. and *P* values from unpaired two-tailed *t*-tests are shown. **c,** Differentiation of E13.5 foetal liver (c-KIT^{+}) progenitors into burst forming units-erythrocyte (BFU-E). Mean ± s.e.m. and *P* values from unpaired two-tailed *t*-tests are reported. **d,** Percentage of haematopoietic progenitors negative for mature lineage markers (Lin^{-}) and SCA-1^{+}c-KIT^{+} (LSK) and SCA-1^{-}c-KIT^{+} (LK) in E13.5 foetal livers with the indicated genotypes. Mean ± s.e.m. and *P* values from unpaired two-tailed *t*-tests are reported. **e,** Mendelian frequencies obtained from inter-crossing *Ripk1*$^{-/-}$*Ripk3*$^{-/-}$*Caspase-8*$^{-/-}$*Hoil-1*$^{+/-}$ mice. **f,** Representative images of mice of the indicated genotypes quantified in (e). **g,** Cytokine levels in embryo homogenates with the indicated genotypes. Mean ± s.e.m and *P* values from one-way ANOVA are reported.

MATERIALS AND METHODS

Mice

The *Hoil-1* floxed (*Hoil-1*$^{fl/fl}$) mice were generated by a gene targeting strategy in ES cells in which the targeting cassette was composed of a hygromycin resistance cassette flanked by *Frt* sites and exons 1 and 2 of the *Hoil-1* gene flanked by *loxP* sites. Southern blots of C57BL/6 ES cell clones containing the homologous recombination were analysed for the specificity of the recombination and the absence of any unwanted integration. Two ES cell clones were used to generate mutant animals on the C57BL/6 genetic background, corresponding to the two independent *Hoil-1*$^{-/-}$ strains (*Hoil-1*$^{-/-}$ and C20*Hoil-1*$^{-/-}$). The hygromycin cassette was removed by crossing these mice with C57BL/6 mice expressing the FlpE recombinase and this was followed by a cross with C57BL/6 mice to remove the flpe transgene. *Hoip*$^{-/-}$ and *Hoil-1*$^{-/-}$ mice were generated by crossing *Hoip*$^{fl/fl}$, mice, previously described[24], and *Hoil-1*$^{fl/fl}$ mice (described here) with transgenic mice expressing the loxP-deleter Cre recombinase (purchased from JAX: 6054, B6.C-Tg(CMV-Cre)1 Cgn/J). Transgenic mice expressing the Cre recombinase under the control of the Tie2 promoter (*Tie2*-Cre) (B6.Cg-Tg(Tek-cre)1Ywa/J)[25] were used to delete floxed genes specifically in endothelial cells. C57BL/6 *Mlkl*$^{-/-}$ mice crossed to *cpdm* mice were previously described[26]. For all other crosses *Mlkl*$^{-/-}$ mice were generated using Transcription activator-like effector nuclease (TALEN). In brief, TALENs targeting exon 1 of the *Mlkl* gene were cloned via Golden-gate assembly. The RVD sequence of TAL1 against TACCGTTTCAGATGTCA was NI HD HD NN NG NG NG HD NI NN NI NG NN NG HD NI and TAL2 against TCGATCTTCCTGCTGCC was HD NN NI NG HD NG NG HD HD NG NN HD NG NN HD HD. Capped RNA was produced *in vitro* using mMESSAGE mMACHINE® T7 Transcription Kit (Ambion) and poly A tail was added using Poly(A) Tailing Kit (Ambion). Purified transcripts were mixed and adjusted to 25 ng/µL. C57BL/6 fertilised eggs were injected into both the cytoplasm and the pro-nucleus. Embryos were transferred into C57BL/6 pseudo-pregnant females. Pups were genotyped by sequencing using genomic DNA obtained from ear punches. One female carrying a 19 bp homozygous deletion causing a premature stop codon was selected for further breeding. *Mlkl*$^{-/-}$ mice were backcrossed to C57BL/6 mice for two generations. *Sharpin*$^{m/m}$ (C57BL/Ka, *cpdm*) and *Tnfr1*$^{-/-}$ (2818, B6.129-Tnfrsf1atm1Mak/J) mice were purchased from JAX. *Tnf*$^{-/-}$ mice (C57BL/6;129S6) were provided by William Kaiser. *Ripk3*$^{-/-}$ [27], *Caspase-8*$^{-/-}$ [28], *Ripk1*^{K45A} [4] and *Ripk1*$^{-/-}$ [29] mice have been reported previously. Timed matings were performed as previously described[8]. All mice were genotyped by PCR, fed *ad libitum.* All animal experiments were conducted under an appropriate UK project license in accordance with the regulations of UK home office for animal welfare according to ASPA (animal (scientific procedure) Act 1986). The relevant Animal Ethics Committee approved all experiments involving *cpdm* and the *Ripk1*$^{-/-}$ crosses which were maintained under appropriate licenses and subject to ethical review at The Walter and Eliza Hall

Institute (Melbourne, Australia) and UT Health Sciences Center San Antonio (TX, USA), respectively.

Histological analysis, TUNEL and immunofluorescence staining

Embryos or organs from adult mice were collected and fixed in 10% buffered formalin and paraffin embedded. Sections of 4 µm were stained with haematoxylin and eosin following standard procedures. Necropsy of adult mice or six sagittal serial sections of two different planes of the embryo were used for blinded pathological analysis. For TUNEL staining, sections were treated according to the manufacturer's instructions (DeadEnd™ Fluorometric TUNEL System, Promega, G3250). For whole mount TUNEL staining and immunofluorescence staining, samples were processed using the ApoTag plus Peroxidase *In Situ* Apoptosis Detection Kit (Millipore, S7101) according to the manufacturer's instructions and as previously described[8]. Quantitation was performed by an experimenter blinded to the genotype of the mice by using ImageJ Software on monochrome images of the whole yolk sac by measuring the area of positive staining. Alternatively, TUNEL-positive cells were counted on five different fields (10x magnification). Yolk sacs were stained with antibodies against PECAM-1 (BD Biosciences, 5533370 Clone MEC13.3) and cleaved caspase-3 (Cell Signaling, 9664), followed by staining with secondary antibodies, Alexa Fluor 594 Goat anti-Rat IgG and Alexa Fluor 488 Goat anti-Rabbit IgG (Invitrogen, A-11007 and A-11034, respectively), and analysed by fluorescent microscopy. Quantification was performed by an experimenter blinded to the genotype of the mice on ten different fields (10x magnification) per yolk sac.

Microfocus CT scan

Embryos were fixed in 4% paraformaldehyde and potassium triiodide (Lugol's iodine/I2KI, to impart tissue contrast), with a total iodine content of 63.25 mg/mL (iodine mass of $2.49 \times 10{-}4$ mol/mL), in a 1:1 ratio for 8 h before imaging. Prior to scanning, the embryos were washed, wrapped in Parafilm M (Bemis, Oshkosh, WI, USA) and secured in 3% w/v Agar (Sigma-Aldrich, UK) within a low-density plastic cylinder to ensure mechanical stability during scan acquisition. Images were acquired using an XT H 225 ST microfocus-CT scanner with a multimetal target (Nikon Metrology, Tring, UK). Scans were reconstructed using modified Feldkamp filtered back projection algorithms with proprietary software (CTPro3D; Nikon Metrology) and post-processed using VG Studio MAX (Volume Graphics GmbH, Heidelberg, Germany). Soft tissues were analysed by Phong shading of direct volume renderings and plain projections and the vascular system by maximum intensity projections.

Cells

MEFs were isolated from E12.5-E13.5 embryos in accordance with standard procedures and these cells were maintained in DMEM medium supplemented with 10% foetal bovine serum (Sigma).

Transformation was performed by lentiviral infection with the SV40 large T antigen. For reconstitution experiments, the coding sequence of murine HOIP, SHARPIN or HOIL-1 wild-type (WT), the UBL domain of HOIL-1 only (HOIL-1-UBL; AA 1-139), HOIL-1-ΔRBR (AA 1-252), HOIL-1-ΔUBL (AA 140-508), HOIL-1 with inactivating mutations T201A/R208A in the NZF domain (HOIL-1-NZFmut) or HOIL-1 with a point mutation in the catalytic cysteine of the RBR domain (HOIL-1-C458A) was inserted in MSCV vector followed by the internal ribosome entry site (IRES)-GFP sequence. These vectors were retrovirally transduced into MEFs and GFP-positive cells were sorted in a MoFlo cytometer (Beckman Coulter).

Immunoprecipitation

For isolation of the TNFR1-SC, transformed MEFs were stimulated with 3xFlag-2xStrep-TNF at 0.5 µg/mL for 15 min, and controls were left untreated. Cells were subsequently solubilised in lysis buffer (30 mM Tris-HCl [pH 7.4], 150 mM NaCl, 2 mM EDTA, 2 mM KCl, 10% Glycerol, 1% Triton X-100, EDTA-free proteinase inhibitor cocktail (Roche, 5056489001) and 1x phosphatase-inhibitor cocktail 2 (Sigma, P5726-1ML) at 4°C for 30 min. The lysates were cleared by centrifugation, and 3xFlag-2xStrep-TNF (0.5 µg/mL/sample) was added to the untreated samples. Subsequently, the lysates were subjected to anti-Flag immunoprecipitation using M2 antibody coupled sepharose beads (Sigma, A2220-5ML) for 16 h. For FADD immunoprecipitation, transformed MEFs were treated with 20 µM zVAD-fmk (Abcam, ab120487) in the presence or absence of 100 ng/mL 6xHis-TNF for 3 h. Cells were lysed as described above and FADD was immunoprecipitated using anti-FADD antibody (Santa Cruz, sc-5559) and protein G Sepharose Beads (GE healthcare, 17-0618-01) at 4°C for 4 h. For Sharpin immunoprecipitation, anti-Sharpin antibody (ProteinTech, 14626-1-AP) was used. For all immunoprecipitations, the beads were washed three times with lysis buffer. Proteins were eluted in 50 µL of LDS buffer (NuPAGE, Invitrogen) containing 50 mM DTT. Samples were analysed by Western blotting.

Western blot analysis and antibodies

Whole embryos were snap-frozen and homogenised in RIPA buffer (50 mM Tris pH 8.0, 150 mM NaCl, 0.5% sodium deoxycholate, 1% NP-40 and 1xEDTA-free proteinase inhibitor cocktail (Roche, 5056489001) or RIPA buffer with 6M Urea for the experiment in Extended data Fig 7h. Alternatively, cells were washed twice with ice-cold PBS prior to lysis in lysis buffer. Protein concentration of lysates was determined using BCA protein assay (Thermo Scientific). Lysates were subsequently denatured in reducing sample buffer at 95°C for 10 min before separation by SDS-PAGE (NuPAGE) and subsequent analysis by Western blotting using antibodies against HOIL-1[30], HOIP (custom-made, Thermo Fisher Scientific), SHARPIN (ProteinTech, 14626-1-AP), TNFR1 (Abcam, ab19139), Actin (Sigma, A1978), pIκBα (Cell Signaling, 9246), IκBα (Cell Signaling, 9242), cleaved caspase-8 (Cell Signaling, 9429), linear ubiquitin (Merck Millipore, MABS199), RIPK1 (BD, 610459), RIPK3 (Enzo,

ADI-905-242-100), FADD (Assay Design, AAM-121), MLKL (Millipore, MABC604), phospho-MLKL (Abcam, ab196436) and Tubulin (Sigma, T9026).

Cell death analysis by PI staining

Cells were seeded to 80% confluence and were then incubated with 100 ng/mL His-tagged TNF, 1 ug/mL CD95L-Fc, 1 µg/mL isoleucine zipper tagged murine TRAIL (iz-mTRAIL), 100 µg/mL Poly(I:C) HMW (InvivoGen, tlrl-pic), 20 ng/mL IFN-γ (Peprotech, 315-05) or 100 ng/mL LT-α (Thermo Fisher Scientific, 10270-HNAE) for 24 h, unless otherwise indicated. When indicated the following inhibitors were used: 20 µM Z-VAD-FMK (Abcam, ab120487), 10 µM Necrostatin-1s (Biovision, 2263-5). Supernatants and adherent cells were harvested and resuspended in PBS containing 5 µg/mL propidium iodide (PI). PI-positive cells were enumerated by FACS (BD Accuri).

RNA sequencing analysis

E13.5 embryos were snap frozen and RNA was prepared using the RNeasy minikit (Qiagen, 74104) according to the manufacturer's instruction. To generate the library, samples were processed using the KAPA mRNA HyperPrep Kit (p/n KK8580) according to the manufacturer's instructions. Briefly, mRNA was isolated from total RNA using Oligo dT beads to pull down poly-adenylated transcripts. The purified mRNA was fragmented using chemical fragmentation (heat and divalent metal cation) and primed with random hexamers. Strand-specific first strand cDNA was generated using Reverse Transcriptase in the presence of Actinomycin D. The second cDNA strand was synthesised using dUTP in place of dTTP, to mark the second strand. The resultant cDNA was then "A-tailed" at the 3' end to prevent self-ligation and adapter dimerisation. Truncated adaptors, containing a T overhang were ligated to the A-Tailed cDNA. Successfully ligated cDNA molecules were then enriched with limited cycle PCR. Libraries to be multiplexed in the same run were pooled in equimolar quantities, calculated from Qubit and Bioanalyser fragment analysis. Samples were sequenced on the NextSeq 500 instrument (Illumina, San Diego, US) using a 43bp paired end run. Run data were de-multiplexed and converted to fastq files using Illumina's bcl2fastq Conversion Software v2.18 on BaseSpace. Fastq files were then aligned to a reference genome using STAR on the BaseSpace RNA-Seq alignment app v1.1.0. Reads per transcript were counted using HTSeq and differential expression was estimated using the BioConductor package DESeq2 (BaseSpace app v1.0.0). Next, 4 groups of differentially regulated genes were analysed: low and high abundance *Ripk3*$^{-/-}$*Caspase-8*$^{-/-}$*Hoil-1*$^{+/-}$ versus *Mlkl*$^{-/-}$*Caspase-8*$^{-/-}$*Hoil-1*$^{+/-}$ embryos and low and high abundance in *Ripk3*$^{-/-}$*Caspase-8*$^{-/-}$*Hoil-1*$^{-/-}$ versus *Mlkl*$^{-/-}$*Caspase-8*$^{-/-}$*Hoil-1*$^{-/-}$ embryos. To identify genes that were specifically altered in the absence of HOIL-1, the Venny 2.1 software was used to exclude genes that were differentially expressed between *Ripk3*$^{-/-}$*Caspase-8*$^{-/-}$*Hoil-1*$^{+/-}$ and *Mlkl*$^{-/-}$*Caspase-8*$^{-/-}$*Hoil-1*$^{+/-}$ embryos from those between *Ripk3*$^{-/-}$*Caspase-8*$^{-/-}$*Hoil-1*$^{-/-}$ and *Mlkl*$^{-/-}$*Caspase-8*$^{-/-}$*Hoil-1*$^{-/-}$ embryos. Genes that were already differentially expressed between the corresponding HOIL-1-expressing controls (i.e. *Ripk3*$^{-/-}$*Caspase-*

8$^{-/-}$*Hoil-1*$^{+/-}$ and *Mlkl*$^{-/-}$*Caspase-8*$^{-/-}$*Hoil-1*$^{+/-}$ embryos) were excluded from the differentially expressed genes between *Ripk3*$^{-/-}$*Caspase-8*$^{-/-}$*Hoil-1*$^{-/-}$ and *Mlkl*$^{-/-}$*Caspase-8*$^{-/-}$*Hoil-1*$^{-/-}$ embryos. The resulting list of genes (33/85, dark green) was entered in the STRING software (string-db.org) to assess for functional enrichment in biological networks. Gene ontology (GO) terms with false discovery rate (FDR) below 1% are shown.

Flow Cytometry analysis (FACS), colony forming unit assay and macrophage culture

For phenotypic analysis, single-cell suspensions from mechanically dissociated E13.5 foetal livers or a pool of aortas (AGM region) from 3 embryos, were stained for 30 min on ice with various antibody cocktails. The antibodies against the surface markers examined were: CD16/32, clone 93 and 2.4G2 (eBioscience, 45-0161-82 and BD553141), CD135, clone A2F10.1 (BD, 553842), Ly-6A/E, clone D7 (Sca-1) (BD, 558162), CD117 (c-Kit), clone 2B8 (BD, 560185), CD34, clone RAM34 (BD, 562608), mouse Lineage Cocktail, clones 17A2/RB6-8C5/RA3-6B2/Ter-119/M1/70 (Biolegend, 133313 and BD, 561301), CD16/32, clone 2.4G2 (BioXcell, CUS-HB-197), CD11b, clone M1/70 (Biolegend, 101228 and eBioscience, 15-0112-81), CD11c, clone HL3 (BD, 561241), F4/80, clone BM8 (Biolegend, 123110), GR-1, clone RB6-8C5 (Biolegend, 108416 and 108410), CD45, clone 30-F11 (Biolegend, 103128 and Biolegend, 103112), CD3ε, clone, 145-2C11 (Biolegend, 100310), B220, clone RA3-6B2, (Biolegend, 103210), CD71, clone RI7217 (Biolegend, 113807), TER-119, clone TER-119 (Biolegend, 116234) and Fixable Viability Dye (eBioscience, 65-0864-18 and 65-0867-14). The myeloid progenitors were identified in the LK population as CD34^{+}CD16/32^{-} (CMP), CD34^{+}CD16/32^{+} (GMP); CD34^{-}CD16/32^{-} (MEP) Fluorescence minus one (FMO) were used as a gating control. For quantification of absolute number of cells, a defined number of flow cytometric reference beads (Invitrogen) were mixed with the samples before acquisition. Samples were processed either using LSR Fortessa (BD Biosciences) or sorted in a FACSAria FUSION cell sorter (BD Biosciences). Data were analysed with FlowJo 7.6.1 software (Treestar). Cytospin preparations of 10.000 cells/slide of E13.5 foetal liver homogenates were stained by May-Grunwald Giemsa staining and enucleated erythrocytes were quantified blindly as number of cells per HPF using ImageJ Software. For growth of primitive erythroid progenitor cells or all haematopoietic stem cells, 5000 sorted Lineage^{-}c-KIT^{+} E13.5 liver cells were cultured in MethoCult™ SF containing cytokines, including EPO (Stem Cell, M3436) or Mouse Methylcellulose Complete Media (R&D, HSC007), respectively. Colonies were enumerated after 14 days of incubation. For preparation of foetal liver-derived macrophages, equal amounts of E13.5 single cell suspensions were cultured and differentiated for 5 days in DMEM supplemented with 10% FCS plus 20% L929-conditioned medium (as a source of M-CSF) supplemented or not with the indicated inhibitors. Cells were imaged using EVOS Auto cell imaging system and viability was measured using the CellTiter-Glo® Luminescent Cell Viability Assay (Promega, G7572). Alternatively, cells were stained with Hoechst dye and enumerated using Citation cell imaging platform.

Cytokine analysis

Embryo homogenates prepared as described above (*Western blot and antibodies*) were analysed with Proteome Profiler Arrays (Mouse Angiogenesis Array, ARY015, and Mouse Cytokine array Panel A, ARY006 both R&D). ELISA kits used were the CXCL4 (R&D, DY595), CXCL11 (Abcam, ab204519), CXCL10 (R&D, DY466-05), IFN Lambda 2/3 (Pbl assay science, 62830-1), IL-1β (ThermoFisher, BMS6002) and IFN-β ELISA (ThermoFisher, 424001).

Epidermal thickness quantification

Per mouse, 1-2 pieces of skin were taken and epidermal thickness was measured by microscopy using a 20x magnification. Quantification was performed by an experimenter blinded to the genotype of the mice by using the CellSens software with at least 20 measurements per mouse.

Pharmacological inhibition of RIPK1 kinase activity

Mice were fed with rodent chow containing 100 mg/kg of the RIPK1 kinase inhibitor GSK3540547A (GSK'547A) (GlaxoSmithKline LLC) starting a week prior to mating and kept on this diet throughout pregnancy until cesarean section at the indicated time points.

Statistics and reproducibility

Group size was determined based on preliminary data sets. Statistical significance was determined using unpaired, two-tailed parametric Student's t-test. One- or two-way ANOVA with Tukey's multiple comparisons test was applied. 95% Confidence interval was considered for statistics and *P*-values (*P*) of <0.05 was considered significant and indicated with **P*<0.05, ***P*<0.01, ****P*<0.001 and *****P*<0.0001. Multiplicity adjusted *P* values are reported for multiple comparisons. All statistical analyses were performed using Graphpad Prism 6. Statisical transformations for RNAseq was performed with DESeq2 and adjusted *P* values utilised the Benjamini Hochberg test. All in vitro experiments were performed at least twice with similar results. Unless indicated in figure legends in vivo experiments were performed with at least 2 embryos per genotype. At least 3 embryos were considered for statistical testing.

Data availability statement

Additional information on this manuscript can be found in the Extended Data files, Supplementary Figure 1 and Source Data (gels and graphs). Data sets including genes differentially regulated genes between embryo homogenates with different mutations obtained in the RNAseq analysis are displayed in Supplementary Table 1.

Extended Data Figure Legends

Extended data Figure 1. HOIL-1-deficient mice die at mid-gestation

a, Schematic representation of the *Hoil-1* knockout strategy. Solid boxes represent *Hoil-1* exons and grey boxes with a star indicate the targeted exons. Boxes with diagonal and horizontal strips represent LoxP and Frt sites, respectively. **b,** Specificity of gene recombination was assessed by Southern blotting with 5' and 3' probes external to the construct in four clones (14B8, 14F6, 20D7 and 21F7). Digest of the DNA with ApaI, followed by hybridisation with the 3' probe was expected to show a 5700 bp band for the WT allele and a 7700 bp band for the mutant allele. All four clones appeared to have the correct recombination on the 3' side. Digest of the DNA with SphI and hybridisation with the 5' probe was expected to show a 4500 bp WT band and a 6200 bp band for the mutated allele. Clones 14B8, 14F6 and 21F7 appeared to be correctly recombined on the 5' side. Finally, cutting the DNA with ApaI and hybridising with a hygro probe showed a single band in all clones, indicative of a single integration of the construct in all four ES clones. Clones 14B8 and 14F6 were selected for generation of the two *Hoil-1*$^{-/-}$ strains. **c**, PCR analysis of *Hoil-1* wild-type, heterozygous and knockout mice. **d**, Protein levels of HOIL-1, HOIP and SHARPIN in whole embryo lysates (*n*= 3 for *Hoil-1*$^{+/-}$ and *Hoil-1*$^{-/-}$ embryos and *n*=1 for *Hoil-1*$^{+/+}$ embryos). For gel source data (c, d), see Supplementary Figure 1. **e**, Quantification of genotypes of animals obtained from inter-crossing *C20Hoil-1*$^{+/-}$ mice. *indicates dead embryos. **f**, Representative images of *C20Hoil-1*$^{+/-}$ and *C20Hoil-1*$^{-/-}$ embryos from E9.5 to E11.5 as quantified in (e). Scale bar: 2 mm. **g,** Single staining showing vascularisation (PECAM-1, top panel) and apoptosis (cleaved Caspase-3, bottom panel) of yolk sacs. Merged image is shown in Fig. 1c. **h,** Whole-mount TUNEL staining of embryos at the indicated stages (embryo/genotype *n*=2 at E10.5, *n*=8 for *Hoil-1*$^{+/-}$ and *n*=5 for *Hoil-1*$^{-/-}$ at E11.5). Scale bar: 2 mm. **i,** Quantification of genotypes of animals obtained from inter-crossing *Hoil-1*$^{fl/wt}$*Tie2-Cre*+ with *Hoil-1*$^{fl/fl}$*Tie2-Cre*- mice. *indicates dead embryos. **j**, Representative images of embryos with conditional deletion of *Hoil-1* in Tie2-Cre expressing cells as quantified in (i). Scale bar: 2 mm. *: poorly vascularised yolk sac.

Extended data Figure 2. TNFR1 signalling drives cell death and lethality of HOIL-1-deficient mice at mid-gestation.

a, d, Quantification of genotypes of animals obtained from inter-crosses of *Tnf*$^{-/-}$*Hoil-1*$^{+/-}$ (a) and *Tnfr1*$^{-/-}$*Hoil-1*$^{+/-}$ (d) mice. *: dead embryos. **b,** Representative images of embryos quantified in (a) at E10.5 and E15.5, *; poor yolk sac. **c,** Cell death as detected by whole-mount TUNEL staining in yolk sacs at E10.5 (n= 3 embryos/genotype). **e,** Single staining showing vascularisation (PECAM-1, top panel) and apoptosis (cleaved Caspase-3, bottom panel) of yolk sacs. Merged image is shown in Fig. 1g. Scale bar: 50 µm. **f,** Representative images of embryos at E16.5 (*n*=2 for *Tnfr1*$^{-/-}$*Hoil-1*$^{+/-}$ and *n*=4 for *Tnfr1*$^{-/-}$*Hoil-1*$^{-/-}$).

Extended data Figure 3. HOIL-1 is required for optimal TNF-induced NF-kB activation independently of its RBR domain.

a, b, d, Western blot analysis of the indicated proteins in whole-cell lysates from MEFs of the indicated genotypes after they had been stimulated with TNF (or left untreated) for the indicated time points in minutes (min) (a), overexpressing the different LUBAC components (b) or the indicated mutant forms of HOIL-1 (d) (*n*=2 independent experiments). **c**, SHARPIN-IP was performed in *Tnf*$^{-/-}$ *Hoil-1*$^{-/-}$ MEFs reconstituted with HOIL-1 or a combination of HOIP and SHARPIN and analysed by Western blotting (*n*=2 independent experiments). TL: total lysate, EV: empty vector. For gel source data, see Supplementary Figure 1.

Extended data Figure 4. Ablation of the kinase activity of RIPK1 in HOIL-1- or HOIP-deficient embryos prevents cell death and lethality at mid-gestation but not at late gestation.

a, b, Quantification of genotypes of animals obtained after inter-crossing *Ripk1*^{K45A}*Hoil-1*$^{+/-}$ (a) and *Ripk1*^{K45A}*Hoip*$^{+/-}$ (b) mice. *indicates dead embryos. **c,** Representative images of embryos quantified in (b) *; poor yolk sac vascularisation. Scale bar: 2 mm. **d,** Whole-mount TUNEL staining of embryos (*n*=2 embryos). Scale bar: 2 mm. **e,** Single staining showing vascularisation (PECAM-1, top panel) and apoptosis (cleaved (cl.) Caspase-3, bottom panel) of yolk sacs. Merged image is shown in Fig. 3b. **f, g,** Representative images of cell death in different organs (f) and quantification (g) as detected by TUNEL staining at E14.5 (*n*=3 embryos/genotype). Scale bar: 50 μm (f). Mean ± s.e.m. (*n*=3 embryos/genotype) and *P* values from one-way ANOVA are reported (g). **h,** Representative images of H&E staining on whole-embryo paraffin sections (*n*=3 embryos/genotype). *; pericardial effusion, n, necrotic area. H, heart; L, lung; Li, liver. Scale bar: 200 μm. **i,** Cell death was analysed by PI staining in MEFs stimulated or not with TNF for 24 h plus the indicated cell death inhibitors. Mean ± s.e.m. (*n*=3 independent experiments) and *P* values from two-way ANOVA are reported.

Extended data Figure 5. Individual deletion of mediators of apoptosis or necroptosis does not prevent cell death and lethality at mid-gestation of HOIL-1- or HOIP-deficient embryos.

a, Western blot analysis of MLKL expression in the indicated organs derived from control *Mlkl*$^{-/-}$ mice (*n*=2 mice/genotype). For gel source data, see Supplementary Figure 1. **b, d, e, f,** Representative images of embryos at different stages of gestation (E10.5: *n*=7 for *Ripk3*$^{-/-}$*Hoil-1*$^{+/-}$ and *n*=5 for *Ripk3*$^{-/-}$ *Hoil-1*$^{-/-}$; E11.5: *n*=5 for *Ripk3*$^{-/-}$*Hoil-1*$^{+/-}$ and *n*=2 for *Ripk3*$^{-/-}$*Hoil-1*$^{-/-}$; E12.5: *n*=9 for *Ripk3*$^{-/-}$*Hoil-1*$^{+/-}$ and *n*=2 for *Ripk3*$^{-/-}$*Hoil-1*$^{-/-}$ (b), E10.5: *n*=16 for *Mlkl*$^{-/-}$*Hoip*$^{+/-}$ and *n*=6 for *Mlkl*$^{-/-}$*Hoip*$^{-/-}$; E11.5: *n*=8 for *Mlkl*$^{-/-}$*Hoip*$^{+/-}$ and *n*=6 for *Mlkl*$^{-/-}$*Hoip*$^{-/-}$; E12.5: *n*=10 for *Mlkl*$^{-/-}$*Hoip*$^{+/-}$ and *n*=5 for *Mlkl*$^{-/-}$*Hoip*$^{-/-}$ (d), E10.5: *n*=5 for *Caspase-8*$^{+/-}$*Hoip*$^{+/-}$ and *n*=4 for *Caspase-8*$^{+/-}$*Hoip*$^{-/-}$; E11.5: *n*=6 for *Caspase-8*$^{+/-}$ *Hoip*$^{+/-}$ and *n*=3 for *Caspase-8*$^{+/-}$*Hoip*$^{-/-}$; E12.5: *n*=3 for *Caspase-8*$^{+/-}$*Hoip*$^{+/-}$ and *n*=2 for *Caspase-8*$^{+/-}$ *Hoip*$^{-/-}$ (e), E10.5: *n*=2 for *Caspase-8*$^{+/-}$*Hoil-1*$^{+/-}$ and *n*=4 for *Caspase-8*$^{+/-}$*Hoil-1*$^{-/-}$; E11.5: *n*=2 for

Caspase-8$^{+/-}$*Hoil-1*$^{+/-}$ and *n*=5 for *Caspase-8*$^{+/-}$*Hoil-1*$^{-/-}$; E12.5: *n*=6 for *Caspase-8*$^{+/-}$*Hoil-1*$^{+/-}$ and *n*=3 for *Caspase-8*$^{+/-}$*Hoil-1*$^{-/-}$ (f)). *: poor yolk sac vascularisation. Scale bar: 2 mm. **c,** Representative images of yolk sac vascularisation and cell death at E10.5 as detected by PECAM-1 (red) and cleaved (cl.) Caspase-3 staining (green) (top panel) and whole mount TUNEL staining (bottom panel) (*n*=4 per genotype). Scale bar: 50 µm.

Extended data Figure 6. Combined deletion of RIPK3 and Caspase-8 prevents cell death but not embryonic lethality at late gestation that is caused by the loss of HOIL-1.

a, Quantification of genotypes of animals obtained from inter-crosses of *Ripk3*$^{-/-}$*Caspase-8*$^{+/-}$*Hoil-1*$^{+/-}$ with *Ripk3*$^{-/-}$*Caspase-8*$^{-/-}$*Hoil-1*$^{+/-}$ mice (left panel) or *Ripk3*$^{-/-}$*Caspase-8*$^{-/-}$*Hoil-1*$^{+/-}$ mice (right panel). **b,** Health status of *Ripk3*$^{-/-}$*Caspase-8*$^{+/-}$*Hoil-1*$^{-/-}$ and *Ripk3*$^{-/-}$*Caspase-8*$^{-/-}$*Hoil-1*$^{-/-}$ embryos at different developmental stages. **c**, Single staining showing vascularisation (PECAM-1, top panel) and apoptosis (cleaved (cl.) Caspase-3, bottom panel) of yolk sacs. Merged image is shown in Fig. 3f. Scale bar: 50 µm. **d,** Cell death as detected by whole-mount TUNEL staining in yolk sacs at E14.5 (left panel) and respective quantification (right panel). Mean ± s.e.m. (*n*=3 embryos/genotype) and *P* values from one-way ANOVA are reported. **e, f** Representative images (e) and quantification (f) of cell death in different organs as detected by TUNEL staining at E13.5 (*n*=3 embryos/genotype) and E14.5 (*n*=5 for *Ripk3*$^{-/-}$*Caspase-8*$^{-/-}$*Hoil-1*$^{+/-}$, *n*=2 for *Ripk3*$^{-/-}$*Caspase-8*$^{-/-}$*Hoil-1*$^{-/-}$ and *Ripk3*$^{-/-}$*Caspase-8*$^{-/-}$*Hoil-1*$^{-/-}$ lung and liver and *n*=3 *Ripk3*$^{-/-}$*Caspase-8*$^{-/-}$*Hoil-1*$^{-/-}$ heart). Scale bar: 50 µm (e). Mean ± s.e.m. values are shown (f). **g,** Cell death was analysed by PI staining in MEFs stimulated or not with the indicated ligands for 24 h. Mean ± s.e.m. (*n*=3 independent experiments) and *P* values from two-way ANOVA are reported. **h,** Representative images of H&E staining on E13.5 whole-embryo paraffin embedded sections (*n*=3 for *Ripk3*$^{-/-}$*Caspase-8*$^{-/-}$*Hoil-1*$^{+/-}$ and *Ripk3*$^{-/-}$*Caspase-8*$^{-/-}$*Hoil-1*$^{-/-}$ and *n*=2 for *Ripk3*$^{-/-}$*Caspase-8*$^{+/-}$*Hoil-1*$^{-/-}$). *: pericardial effusion, arrows; congested vessels H, heart; L, lung; Li, liver. Scale bar: 200 µm. **i,** Representative images of micro-focus CT scan images of whole E13.5 embryos (*n*=3 embryos/genotype). *: pericardial effusion

Extended data Figure 7. Combined deletion of MLKL and Caspase-8 promotes survival of LUBAC-deficient mice.

a, Quantification of genotypes of animals obtained from inter-crosses of *Mlkl*$^{-/-}$*Caspase-8*$^{+/-}$*Hoip*$^{+/-}$ with *Mlkl*$^{-/-}$*Caspase-8*$^{-/-}$*Hoip*$^{+/-}$ mice. *: dead embryos. **b,** Representative images of adult mice as quantified in (a). **c,** Kaplan-Meier plot of mouse survival (*n*=6 for *Mlkl*$^{-/-}$*Caspase-8*$^{-/-}$*Hoip*$^{-/-}$ and *n*=9 for *Mlkl*$^{-/-}$*Caspase-8*$^{-/-}$*Hoil-1*$^{-/-}$ mice). **d,** Representative images of H&E staining of the indicated organs (*n*=3 mice/genotype). Scale bar: 200 µm. **e,** Representative images of yolk sac vascularisation (PECAM-1, red) and apoptosis (cleaved (cl.) Caspase-3, green) (top panel) at E13.5 and respective quantifications (bottom panel). Mean ± s.e.m (*n*=5 for *Mlkl*$^{-/-}$*Caspase-8*$^{-/-}$*Hoil-1*$^{+/-}$ and *Mlkl*$^{-/-}$*Caspase-*

8$^{-/-}$*Hoil-1*$^{-/-}$ and *n*=2 for *Mlkl*$^{-/-}$*Caspase-8*$^{+/-}$*Hoil-1*$^{-/-}$) are shown and results were analysed with unpaired two-tailed *t*-tests comparing *Mlkl*$^{-/-}$*Caspase-8*$^{-/-}$*Hoil-1*$^{+/-}$ and *Mlkl*$^{-/-}$*Caspase-8*$^{-/-}$*Hoil-1*$^{-/-}$ embryos. **f,** Representative images of H&E staining of the indicated organs (*n*=3 embryos/genotype). Scale bar: 200 µm. **g,** Epidermal thickness quantification of mice of the indicated genotypes in (f). Mean ± s.e.m values (*n*=3 mice/genotype) are shown and results were analysed with unpaired two-tailed *t*-tests. **h,** Western blot analysis of lysates from whole E13.5 embryos of the indicated genotypes as well as L929 cells treated or not with TNF plus zVAD-fmk for 2 h as antibody validation (*n*=4 embryos/genotype performed twice). For gel source data, see Supplementary Figure 1.

Extended data Figure 8. Combined deletion of RIPK3 and Caspase-8 causes haematopoietic defects and RIPK1-dependent embryonic lethality in HOIL-1-deficient mice.

a, Venn diagram depicting genes differentially expressed by RNAseq analysis between E13.5 embryos of the indicated genotypes. **b,** Gene Ontology (GO) enrichment analysis of differentially (85 low and 35 high in (a)) expressed genes. FDR: false discovery rate .**c,** Representative FACS profile of E13.5 foetal liver cells with different erythroblast populations gated according to their CD71 and TER119 expression levels (R1-R5). R1 contains immature RBC progenitors, including BFU-E and CFU-E; R2 comprises mainly pro-erythroblasts and early basophilic erythroblasts; R3 contains both early and late basophilic erythroblasts; R4 is composed of chromatophilic and orthochromatophilic erythroblasts; and R5 consists of late orthochromatophilic erythroblasts and reticulocytes and **q**uantification. Mean ± s.e.m. (*n*=14 *Ripk3*$^{-/-}$*Caspase-8*$^{-/-}$*Hoil-1*$^{+/-}$, *n*=8 *Ripk3*$^{-/-}$*Caspase-8*$^{-/-}$*Hoil-1*$^{-/-}$, *n*=5 for *Mlkl*$^{-/-}$*Caspase-8*$^{-/-}$*Hoil-1*$^{-/-}$ and *n*=3 for *Mlkl*$^{-/-}$*Caspase-8*$^{-/-}$*Hoil-1*$^{-/-}$ foetal livers) and *P* values from two-way ANOVA are reported. **d, h, k** Representative FACS profile of E13.5 foetal liver cells for the indicated haematopoietic populations (sample size specified in (e-g, i, j)). **e, f, j** Total cell number of the different haematopoietic cell subsets in foetal liver cell suspensions from E13.5 embryos of the indicated genotypes gated as in (d), (h) and (k), respectively. Total number of multipotent progenitors (LSK and LK cells) (e), mature CD45$^+$ blood cells, including granulocytes (GR-1$^+$) and macrophages (F4-80$^+$) (f) and myeloid progenitors (CMP, GMP and MEP) (j). Mean ± s.e.m. and *P* values from unpaired two-tailed *t*-tests are reported. **g, i,** Percentages of mature CD45$^+$ leucocytes, GR-1$^+$ and F4-80$^+$ cells (g) and CMP, GMP and MEP (i). Mean ± s.e.m. and *P* values from unpaired two-tailed *t*-tests are reported. **l,** Differentiation of E13.5 foetal liver (c-KIT$^+$) progenitors into CFU-granulocytes and macrophages (GM), burst forming units-erythrocyte (BFU-E) or and CFU-granulocyte, erythroid, macrophage, megakaryocyte (GEMM). Mean ± s.e.m. (*n*=2 foetal livers). **m**, Micrographs of differentiated macrophages (*n*=3 *Ripk3*$^{-/-}$*Caspase-8*$^{-/-}$*Hoil-1*$^{+/-}$ and *Ripk3*$^{-/-}$*Caspase-8*$^{-/-}$*Hoil-1*$^{-/-}$, *n*=5 *Mlkl*$^{-/-}$*Caspase-8*$^{-/-}$*Hoil-1*$^{+/-}$ and *n*=4 *Mlkl*$^{-/-}$*Caspase-8*$^{-/-}$*Hoil-1*$^{-/-}$ foetal livers) and percentage viability of macrophages from E13.5 foetal liver cell suspensions from embryos of the

indicated genotypes in the presence or absence of the indicated inhibitors as measured by Cell Titer Glo. Mean ± s.e.m. (*n*=3 *Ripk3*$^{-/-}$*Caspase-8*$^{-/-}$*Hoil-1*$^{+/-}$ and *Ripk3*$^{-/-}$*Caspase-8*$^{-/-}$*Hoil-1*$^{-/-}$, *n*=5 *Mlkl*$^{-/-}$ *Caspase-8*$^{-/-}$*Hoil-1*$^{+/-}$ and *n*=4 *Mlkl*$^{-/-}$*Caspase-8*$^{-/-}$*Hoil-1*$^{-/-}$ foetal livers) and *P* values from two-way ANOVA are reported. **o**, MicroCT scan images of *Ripk3*$^{-/-}$*Caspase-8*$^{-/-}$*Hoil-1*$^{-/-}$ embryos showing maximum intensity projections, with windowing applied to highlight vasculature (high contrast). No anatomical defects that would explain destruction of RBCs or poor distribution of blood to the peripheries were found (*n*=3 embryos). Left image: yellow star: distal aorta, green star: umbilical vessels and red star: descending thoracic aorta. Right image, yellow star: carotid artery, red star: descending thoracic aorta, white star: ductus arteriosus, blue star: ascending thoracic aorta. **p,** Representative FACS profile of a pool of three E11.5 dorsal aortas, containing the AGM region, per indicated genotype and quantification. This experiment was performed once with 3 embryos per genotype.

Extended data Figure 9. Concomitant deletion of RIPK1 prevents embryonic lethality of *Ripk3*$^{-/-}$ *Caspase-8*$^{-/-}$*Hoil-1*$^{-/-}$ mice.

a, Kaplan-Meier plot of mouse survival (*n*=17 for *Ripk1*$^{-/}$ *Ripk3*$^{-/-}$*Caspase-8*$^{-/-}$*Hoip*$^{-/-}$ and *n*=2 for *Ripk*$^{+/-}$*Ripk3*$^{-/-}$*Caspase-8*$^{-/-}$*Hoip*$^{-/-}$ mice). **b,** Quantification of genotypes of animals obtained from inter-crosses of *Ripk1*$^{+/-}$*Hoil-1*$^{+/-}$ mice. For simplicity not all possible genotypes are represented. **c**, Percentage viability of macrophages from E13.5 foetal liver cell suspensions from embryos of the indicated genotypes as measured by Cell Titer Glo. Mean ± s.e.m. (*n*=5 foetal livers/genotype) are reported and results were analysed with unpaired two-tailed *t*-tests. **d**, Cytokine arrays from *Ripk3*$^{-/-}$ *Caspase-8*$^{-/-}$*Hoil-1*$^{+/-}$ and *Ripk3*$^{-/-}$*Caspase-8*$^{-/-}$*Hoil-1*$^{-/-}$ embryos (left panels) and table listing the altered cytokines (right panel). Red squares highlight the differences (*n*=1 for each genotype). For gel source data, see Supplementary Figure 1. **e**, Cytokine analysis in homogenates from embryos of the indicated genotypes. Mean ± s.e.m. (*n*=3 embryos/genotype) and *P* values from one-way ANOVA are reported. **f,** Representative images of E16.5 embryos from control mothers or mothers fed with the RIPK1 kinase inhibitor GSK'457A from mating and throughout gestation (embryos treated with GSK'457A *n*=5 for *Ripk3*$^{-/-}$*Caspase-8*$^{-/-}$*Hoil-1*$^{+/-}$ and *n*=7 *Ripk3*$^{-/-}$*Caspase-8*$^{+/-}$*Hoil-1*$^{-/-}$ and *n*=3 for *Ripk3*$^{-/-}$*Caspase-8*$^{-/-}$*Hoil-1*$^{-/-}$). Scale bar: 5 mm.

Extended data Figure 10. Schematic representation of findings in this study

a, Diagram indicating extent of viability and phenotypes of single, double, triple and quadruple knockout mice. Red lines indicate cell death and loss of yolk sac vascularisation phenotype. Green line indicates mild cell death phenotype without loss of yolk sac vascularisation. Asterisk (*) indicates that heart defects were observed. **b,** Proposed model of LUBAC function during embryogenesis. At mid-gestation (left panel), LUBAC maintains vascular tissue integrity by preventing aberrant

TNF/LT-α-mediated Caspase-8- and RIPK3/MLKL-induced cell death. At late gestation, LUBAC is not only required to prevent aberrant cell death but also to prevent severe defects in haematopoiesis that are driven by RIPK1 but can be prevented by RIPK3 (middle panel). Genetic ablation of LUBAC and of different components of the cell death machinery indicates that (right panel): 1) in the absence of LUBAC, Caspase-8 and RIPK3, RIPK1 provokes lethality most likely by depleting multipotent progenitors in the haematopoietic compartment; 2) in the absence of Caspase-8 and MLKL, cell death induced by loss of LUBAC is prevented and RIPK3 is present to exert its protective role on foetal haematopoiesis by precluding aberrant RIPK1 signalling; and 3) in the absence of Caspase-8 and RIPK3, the presence of LUBAC is sufficient to prevent RIPK1 from causing severe defects in haematopoiesis and lethality since *Ripk3*$^{-/-}$*Caspase-8*$^{-/-}$ mice are viable[15,16,23]. This indicates that RIPK3 and LUBAC can compensate for each other to block aberrant RIPK1 signalling.

Figure 1

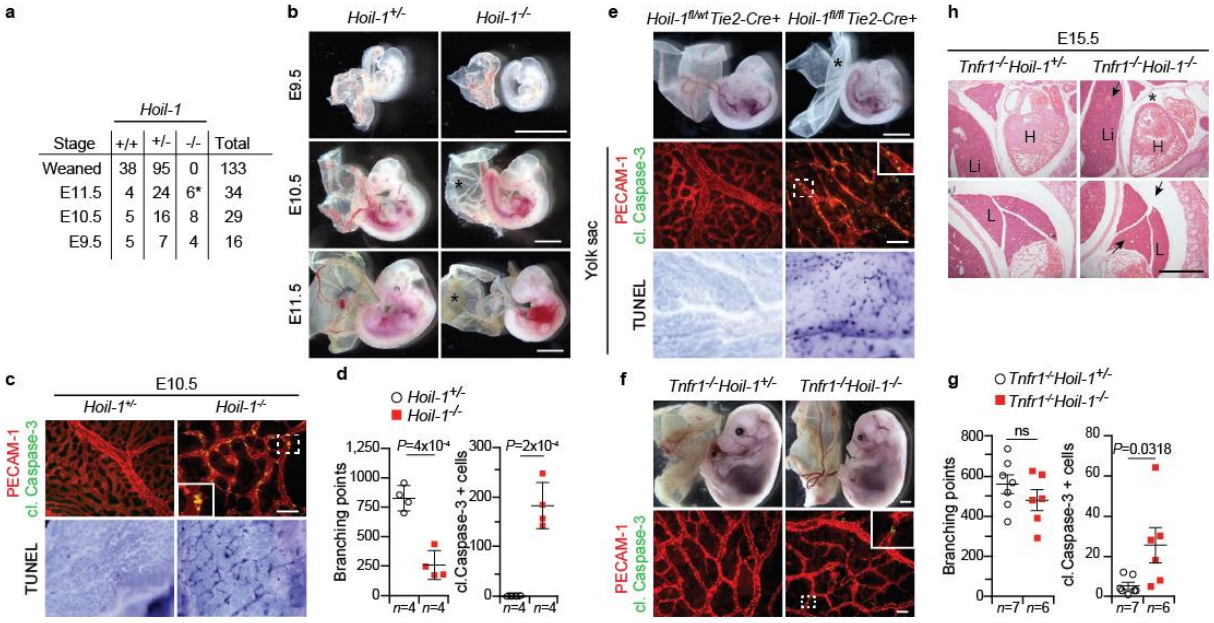
a
Hoil-1
Stage +/+ +/- -/- Total
Weaned 38 95 0 133
E11.5 4 24 6* 34
E10.5 5 16 8 29
E9.5 5 7 4 16
b
Hoil-1+/-
Hoil-1-/-
E9.5
E10.5
E11.5
e
Hoil-1fl/wt Tie2-Cre+
Hoil-1fl/fl Tie2-Cre+
Yolk sac
PECAM-1
cl. Caspase-3
TUNEL
h
E15.5
Tnfr1-/-Hoil-1+/-
Tnfr1-/-Hoil-1-/-
H
Li
L
c
E10.5
Hoil-1+/-
Hoil-1-/-
PECAM-1
cl. Caspase-3
TUNEL
d
Hoil-1+/-
Hoil-1-/-
Branching points
P=4x10-4
cl.Caspase-3 + cells
P=2x10-4
n=4 n=4
f
Tnfr1-/-Hoil-1+/-
Tnfr1-/-Hoil-1-/-
PECAM-1
cl. Caspase-3
g
Tnfr1-/-Hoil-1+/-
Tnfr1-/-Hoil-1-/-
Branching points
ns
cl.Caspase-3 + cells
P=0.0318
n=7 n=6
n=7 n=6

Figure 2

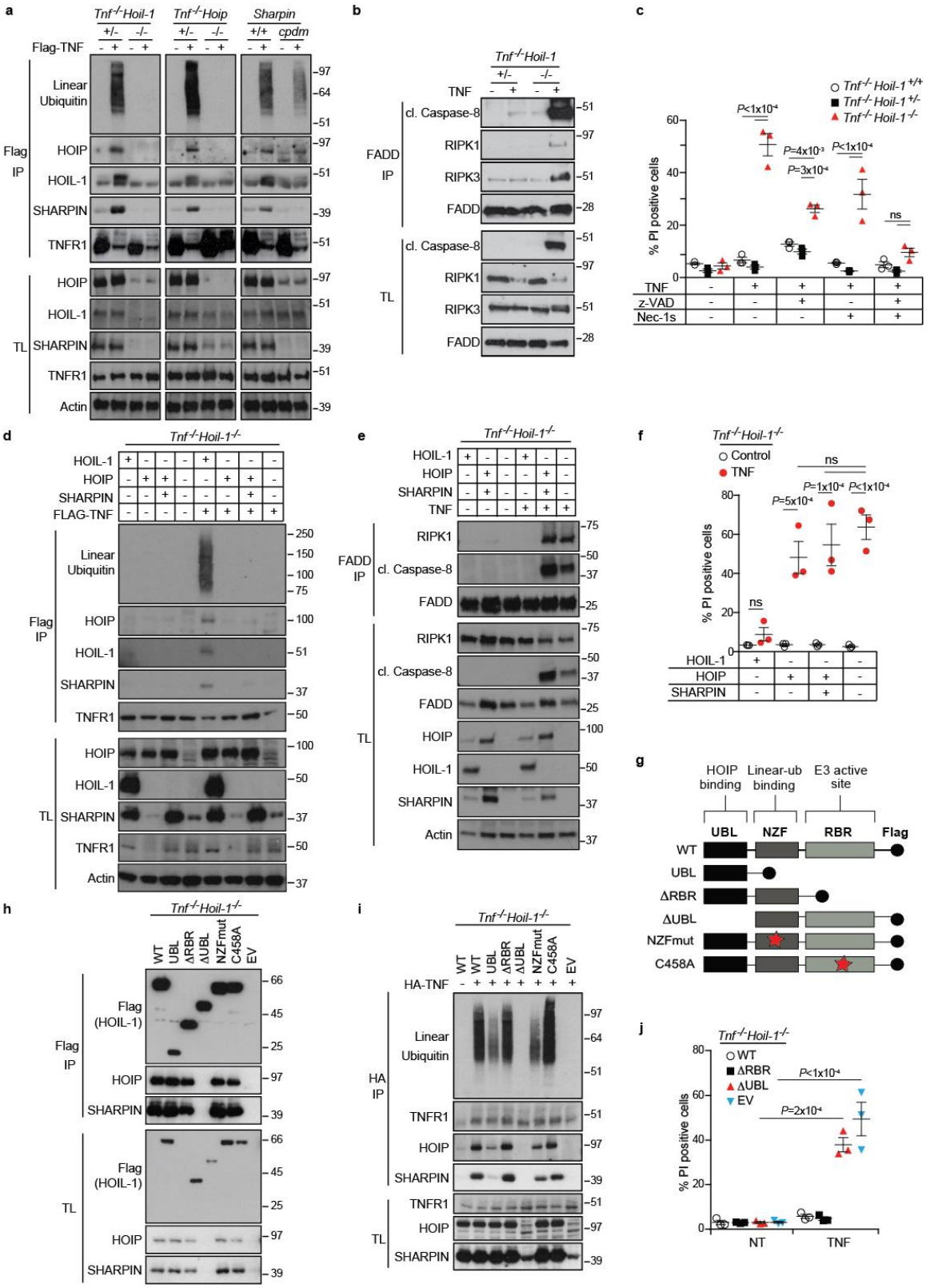
a
Tnf-/-Hoil-1
Tnf-/-Hoip
Sharpin
cpdm
Flag-TNF
Flag IP
Linear Ubiquitin
HOIP
HOIL-1
SHARPIN
TNFR1
TL
Actin
b
Tnf-/-Hoil-1
TNF
FADD IP
cl. Caspase-8
RIPK1
RIPK3
FADD
TL
c
Tnf-/- Hoil-1+/+
Tnf-/- Hoil-1+/-
Tnf-/- Hoil-1-/-
% PI positive cells
P<1x10-4
P=4x10-3
P=3x10-4
ns
TNF
z-VAD
Nec-1s
d
Tnf-/-Hoil-1-/-
HOIL-1
HOIP
SHARPIN
FLAG-TNF
e
Tnf-/-Hoil-1-/-
f
Tnf-/-Hoil-1-/-
Control
TNF
P=5x10-4
P=1x10-4
g
HOIP binding
Linear-ub binding
E3 active site
UBL
NZF
RBR
Flag
WT
UBL
ΔRBR
ΔUBL
NZFmut
C458A
h
Tnf-/-Hoil-1-/-
WT
UBL
ΔRBR
ΔUBL
NZFmut
C458A
EV
Flag (HOIL-1)
i
Tnf-/-Hoil-1-/-
HA-TNF
HA IP
j
Tnf-/-Hoil-1-/-
WT
ΔRBR
ΔUBL
EV
P=2x10-4
NT
TNF

Figure 3

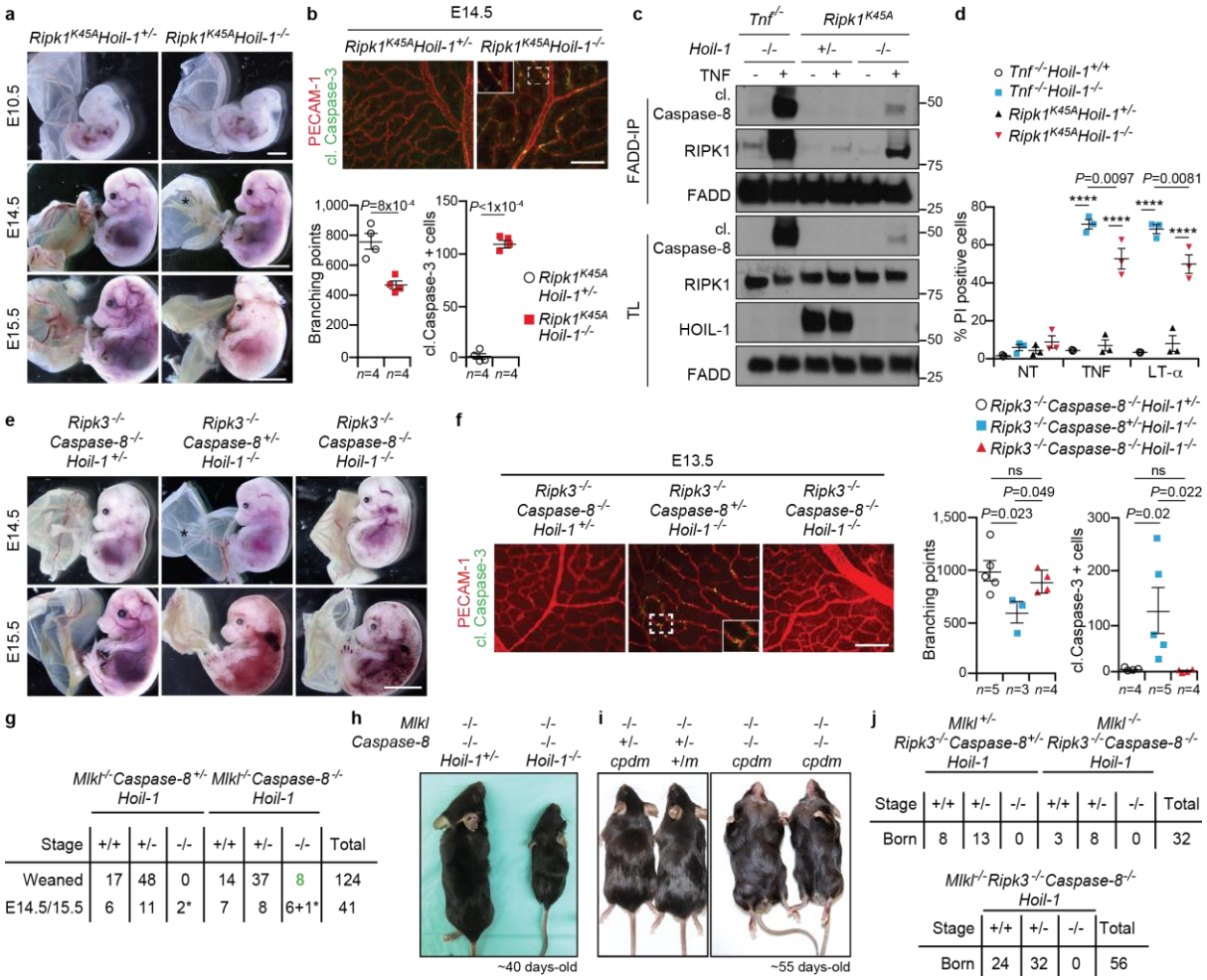

Stage	+/+	+/-	-/-	+/+	+/-	-/-	Total
Weaned	17	48	0	14	37	8	124
E14.5/15.5	6	11	2*	7	8	6+1*	41

Stage	+/+	+/-	-/-	+/+	+/-	-/-	Total
Born	8	13	0	3	8	0	32

Stage	+/+	+/-	-/-	Total
Born	24	32	0	56

Figure 4

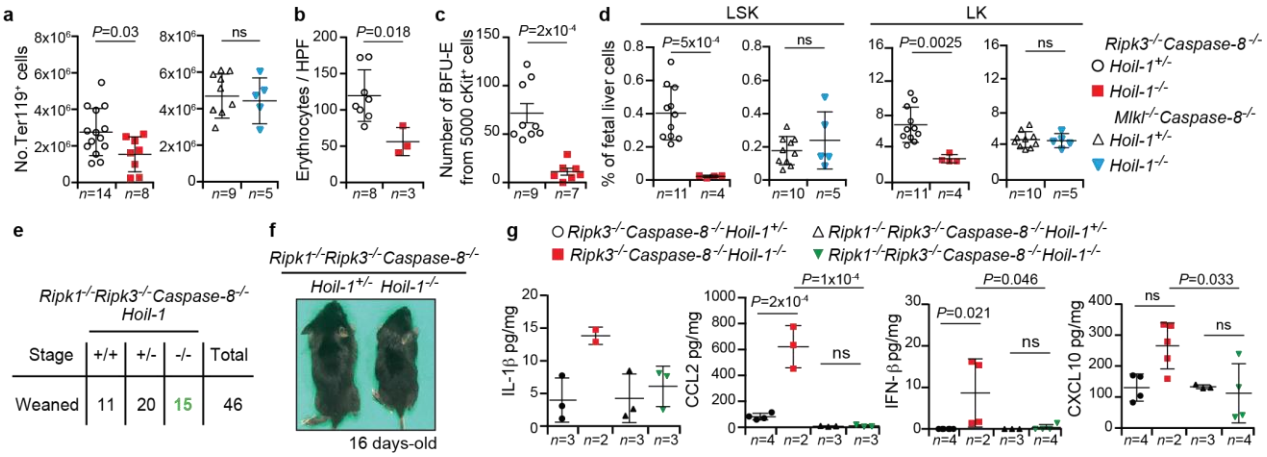
a
No.Ter119+ cells
P=0.03
ns
n=14 n=8 n=9 n=5
b
Erythrocytes / HPF
P=0.018
n=8 n=3
c
Number of BFU-E from 5000 cKit+ cells
P=2x10-4
n=9 n=7
d
LSK
LK
% of fetal liver cells
P=5x10-4
ns
P=0.0025
ns
n=11 n=4 n=10 n=5 n=11 n=4 n=10 n=5
Ripk3-/-Caspase-8-/-
Hoil-1+/-
Hoil-1-/-
Mlkl-/-Caspase-8-/-
Hoil-1+/-
Hoil-1-/-
e
Ripk1-/-Ripk3-/-Caspase-8-/-
Hoil-1
Stage +/+ +/- -/- Total
Weaned 11 20 15 46
f
Ripk1-/-Ripk3-/-Caspase-8-/-
Hoil-1+/- Hoil-1-/-
16 days-old
g
Ripk3-/-Caspase-8-/-Hoil-1+/-
Ripk3-/-Caspase-8-/-Hoil-1-/-
Ripk1-/-Ripk3-/-Caspase-8-/-Hoil-1+/-
Ripk1-/-Ripk3-/-Caspase-8-/-Hoil-1-/-
IL-1β pg/mg
CCL2 pg/mg
P=1x10-4
P=2x10-4
ns
IFN-β pg/mg
P=0.046
P=0.021
ns
CXCL10 pg/mg
P=0.033
ns
ns
n=3 n=2 n=3 n=3 n=4 n=2 n=3 n=3 n=4 n=2 n=3 n=4 n=4 n=2 n=3 n=4

Extended Data Figure 1

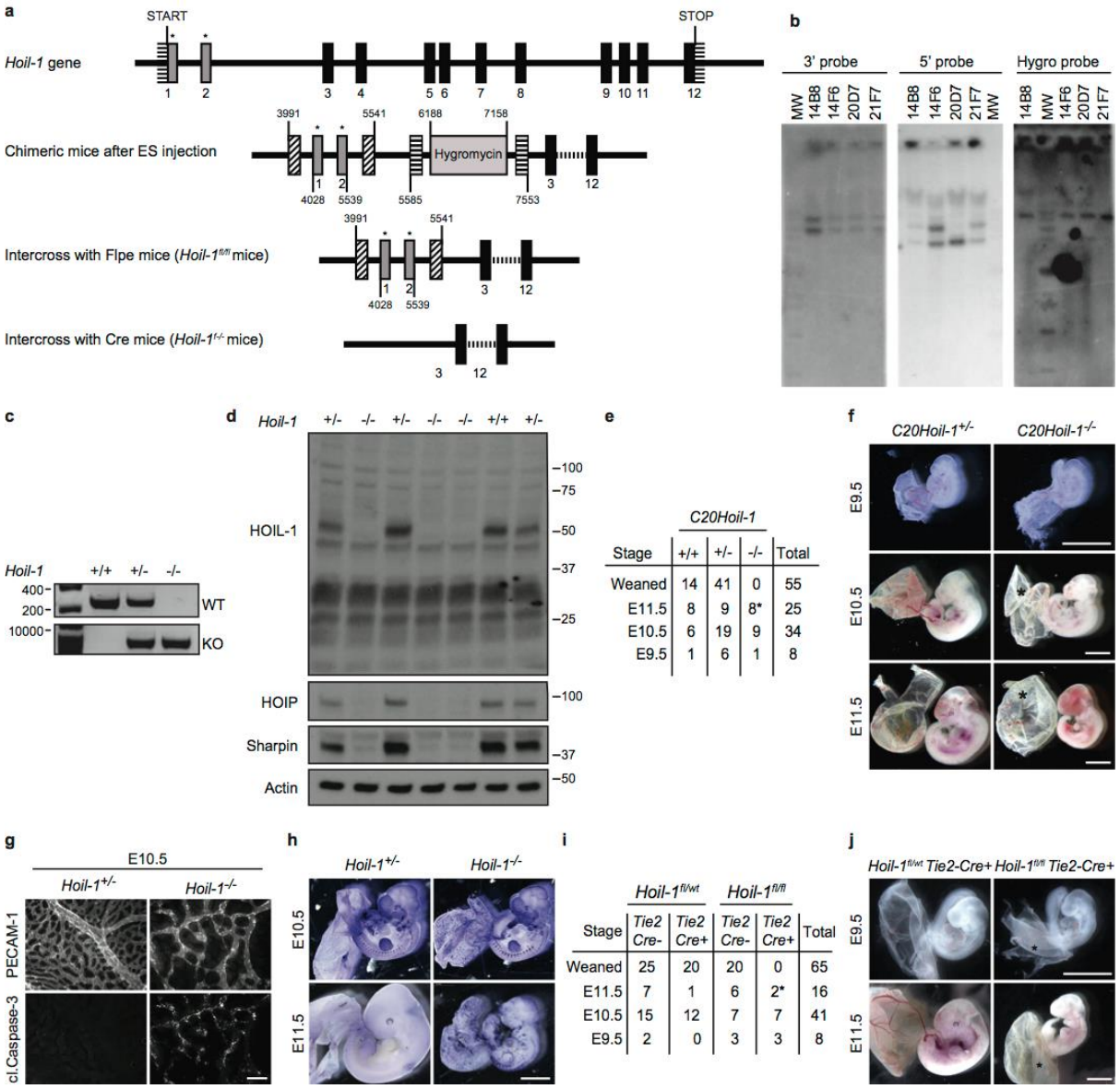

Extended Data Figure 2

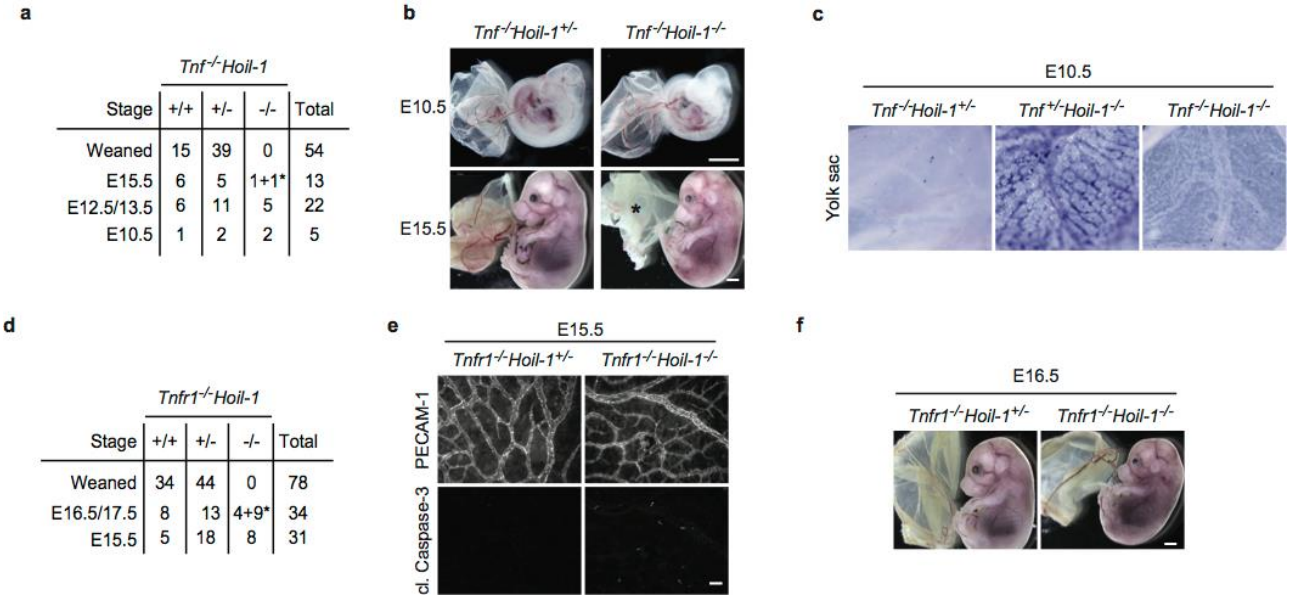

Extended Data Figure 3

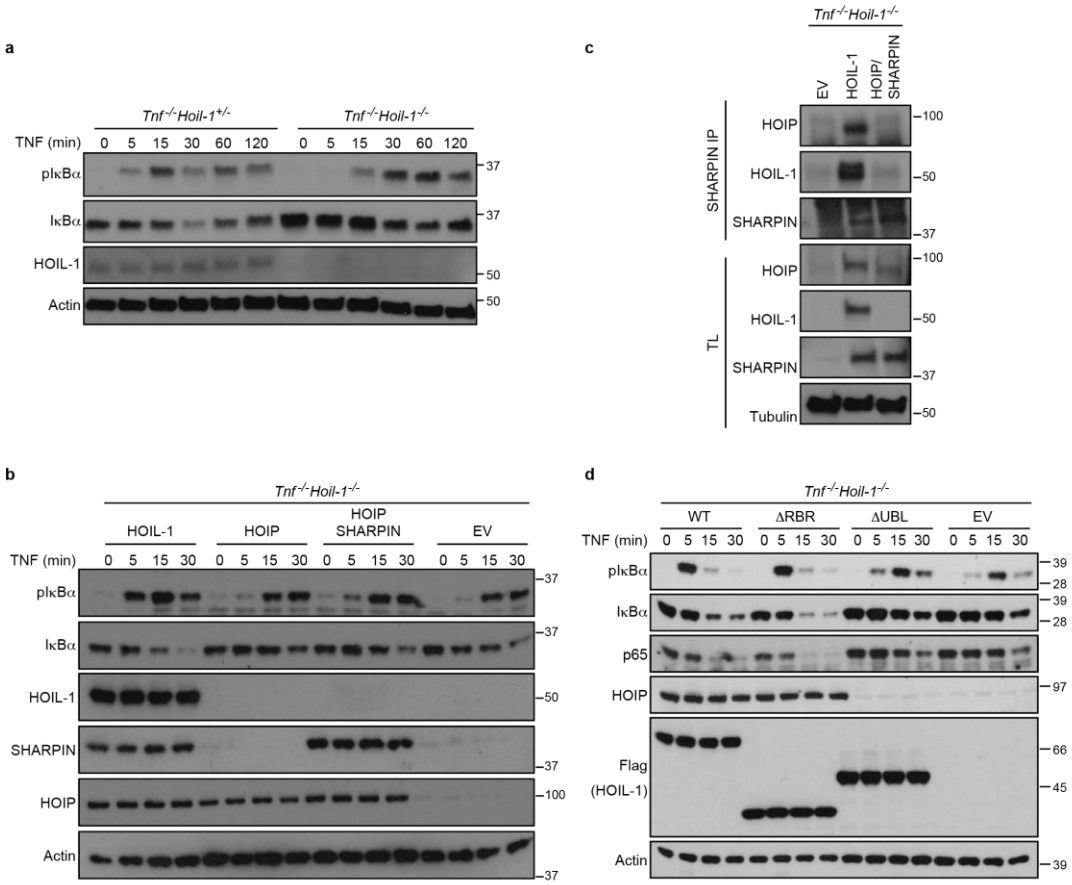

Extended Data Figure 4

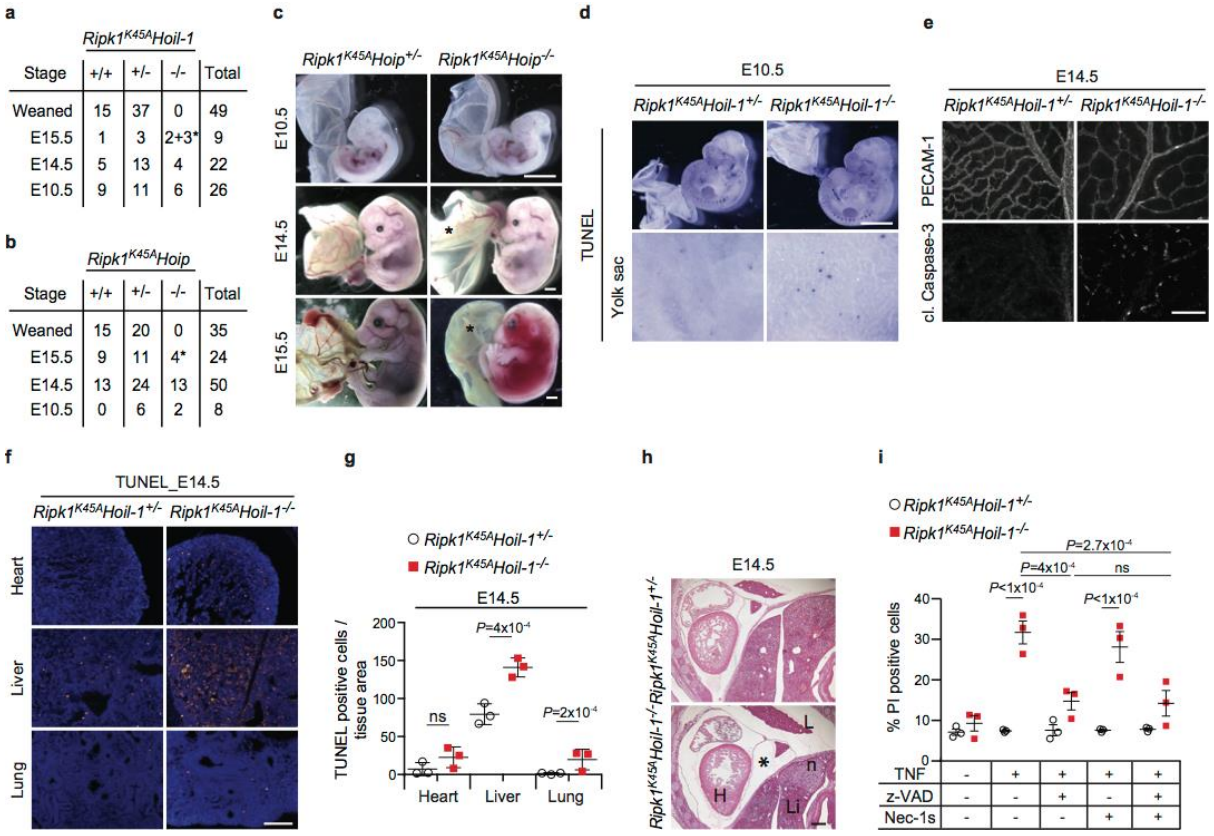

Extended Data Figure 5

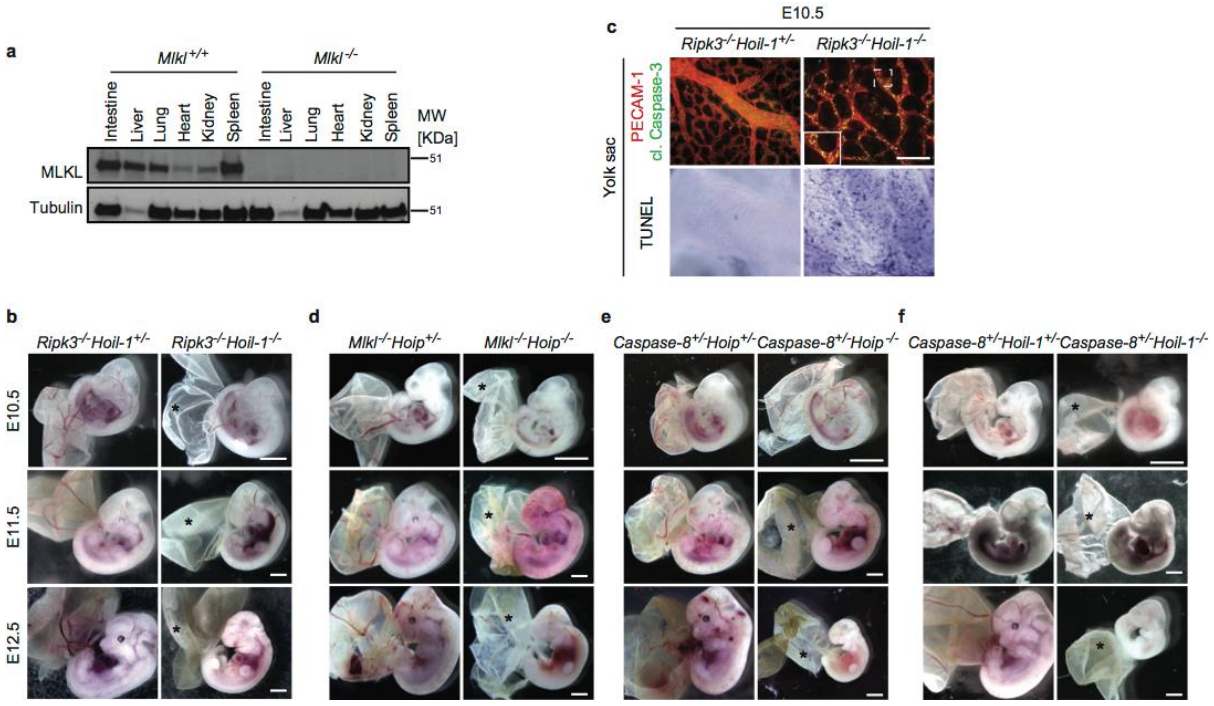

Extended Data Figure 6

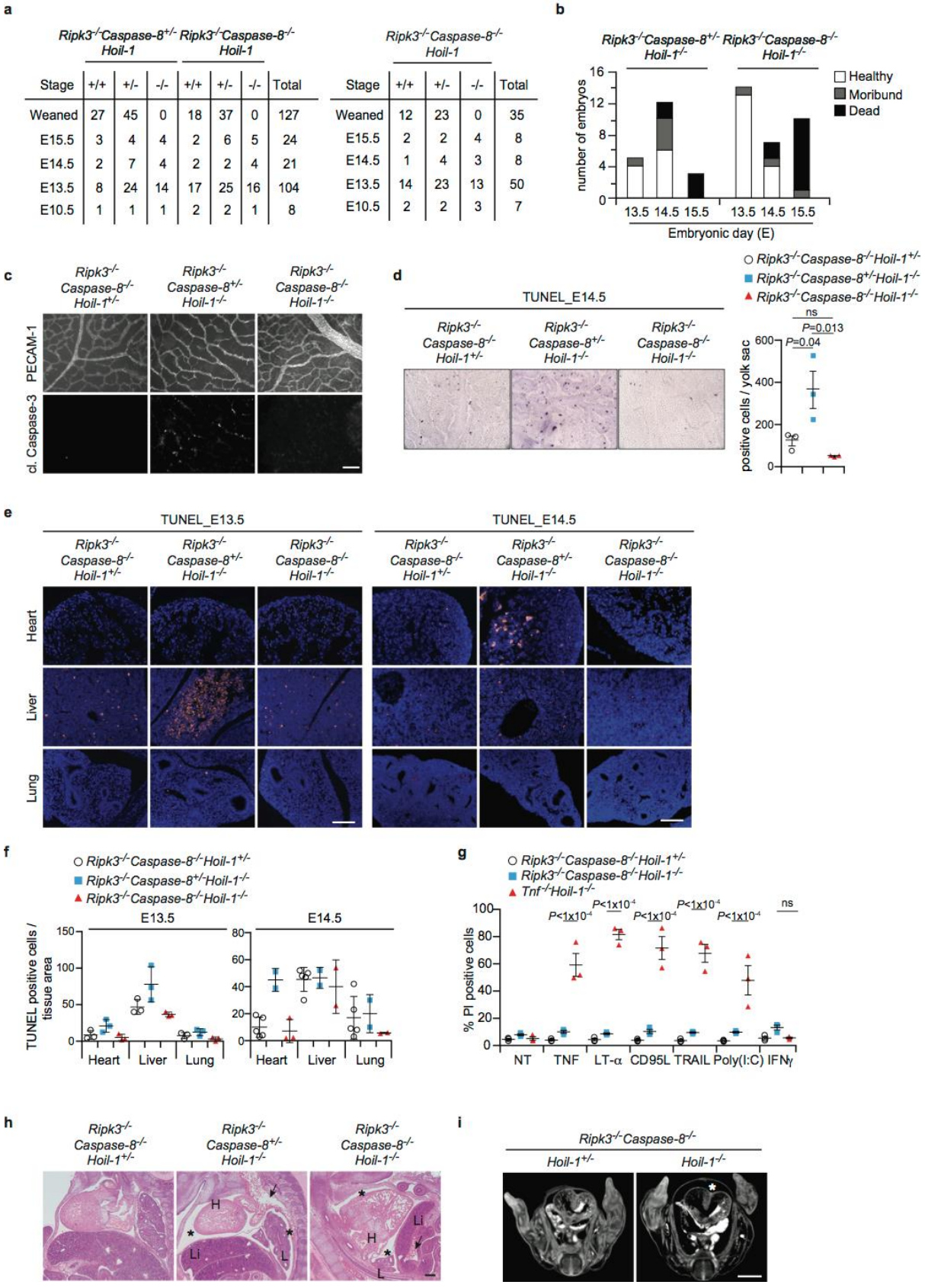

Stage	+/+	+/-	-/-	+/+	+/-	-/-	Total
Weaned	27	45	0	18	37	0	127
E15.5	3	4	4	2	6	5	24
E14.5	2	7	4	2	2	4	21
E13.5	8	24	14	17	25	16	104
E10.5	1	1	1	2	2	1	8

Stage	+/+	+/-	-/-	Total
Weaned	12	23	0	35
E15.5	2	2	4	8
E14.5	1	4	3	8
E13.5	14	23	13	50
E10.5	2	2	3	7

Extended Data Figure 7

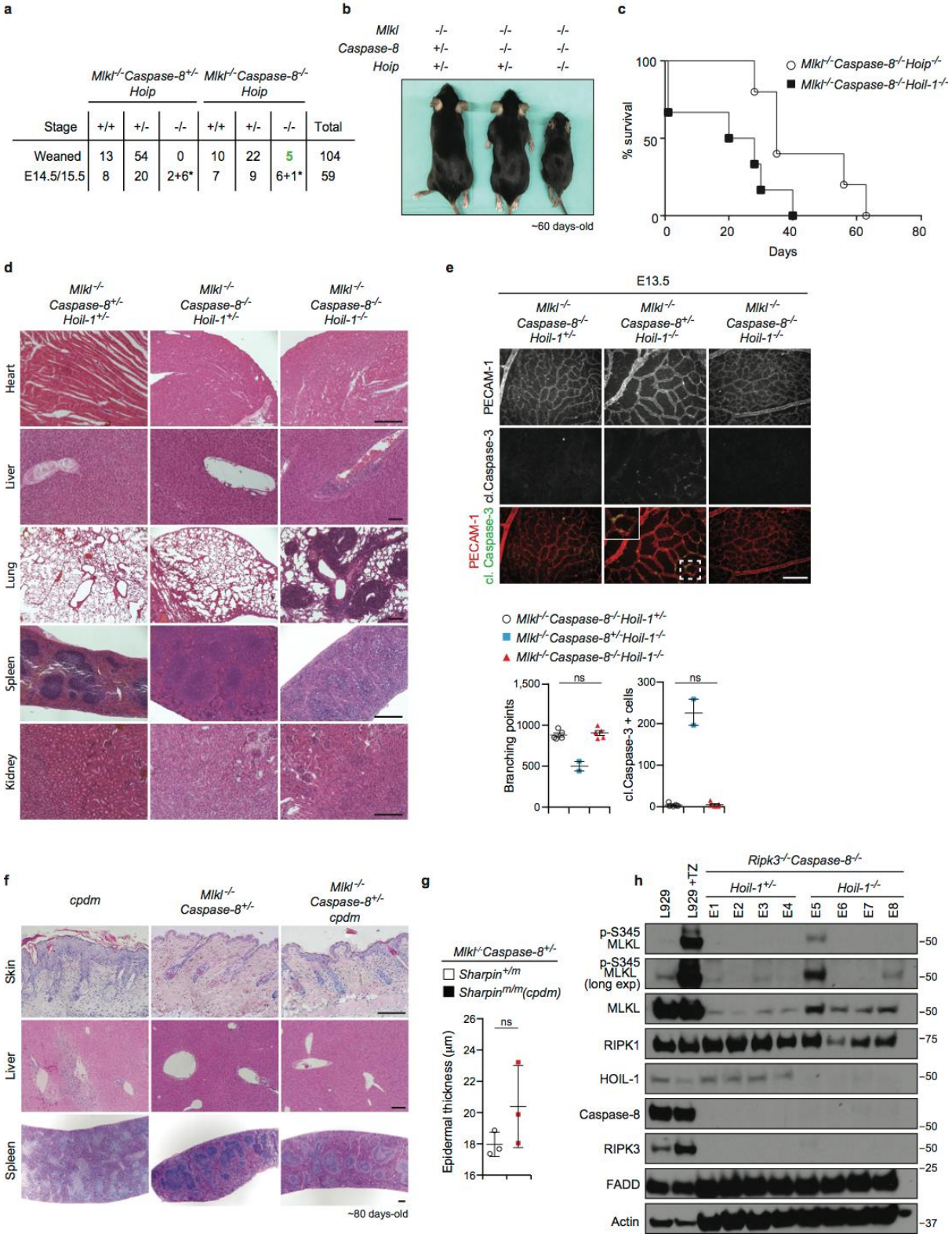

Extended Data Figure 8

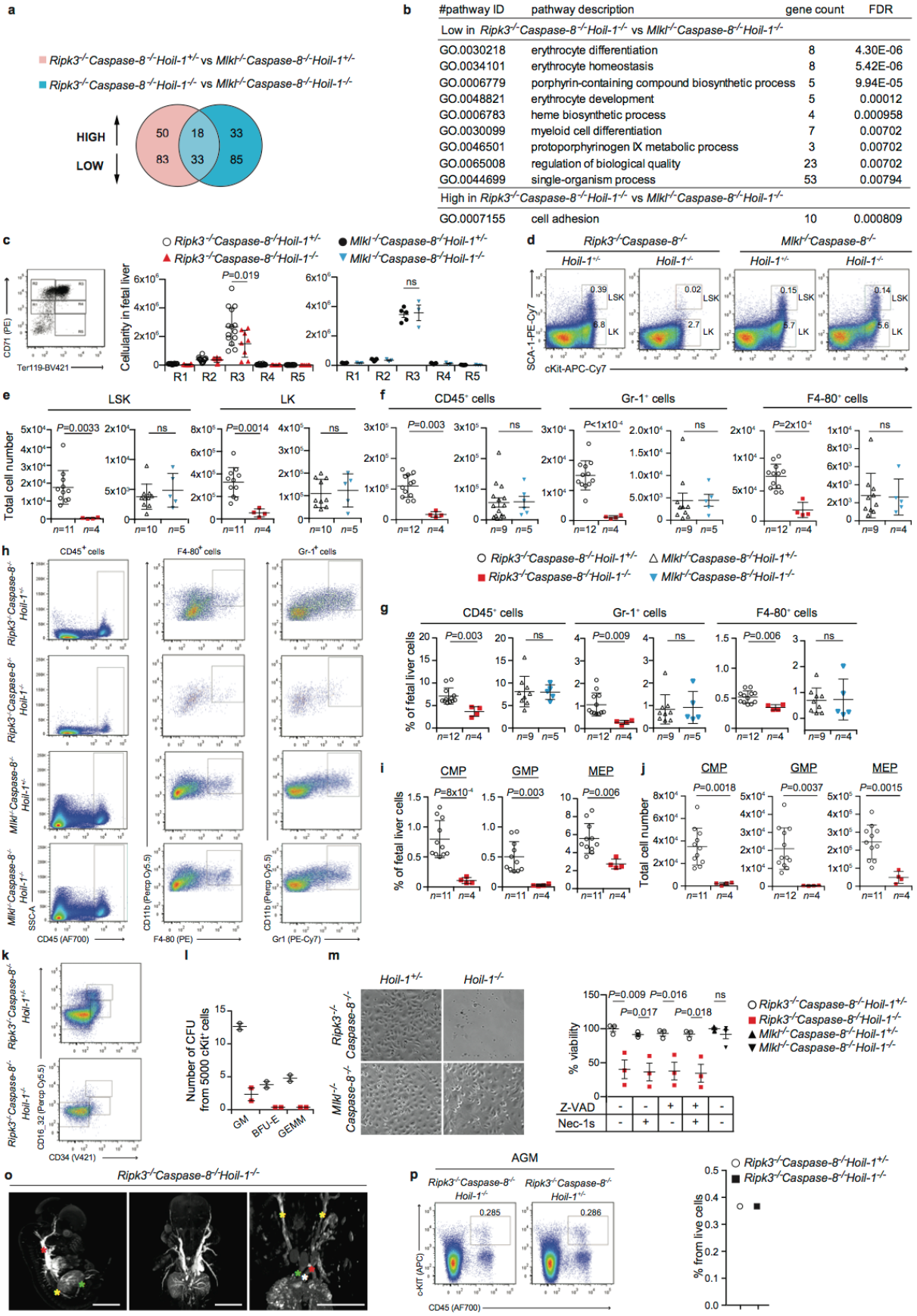

Extended Data Figure 9

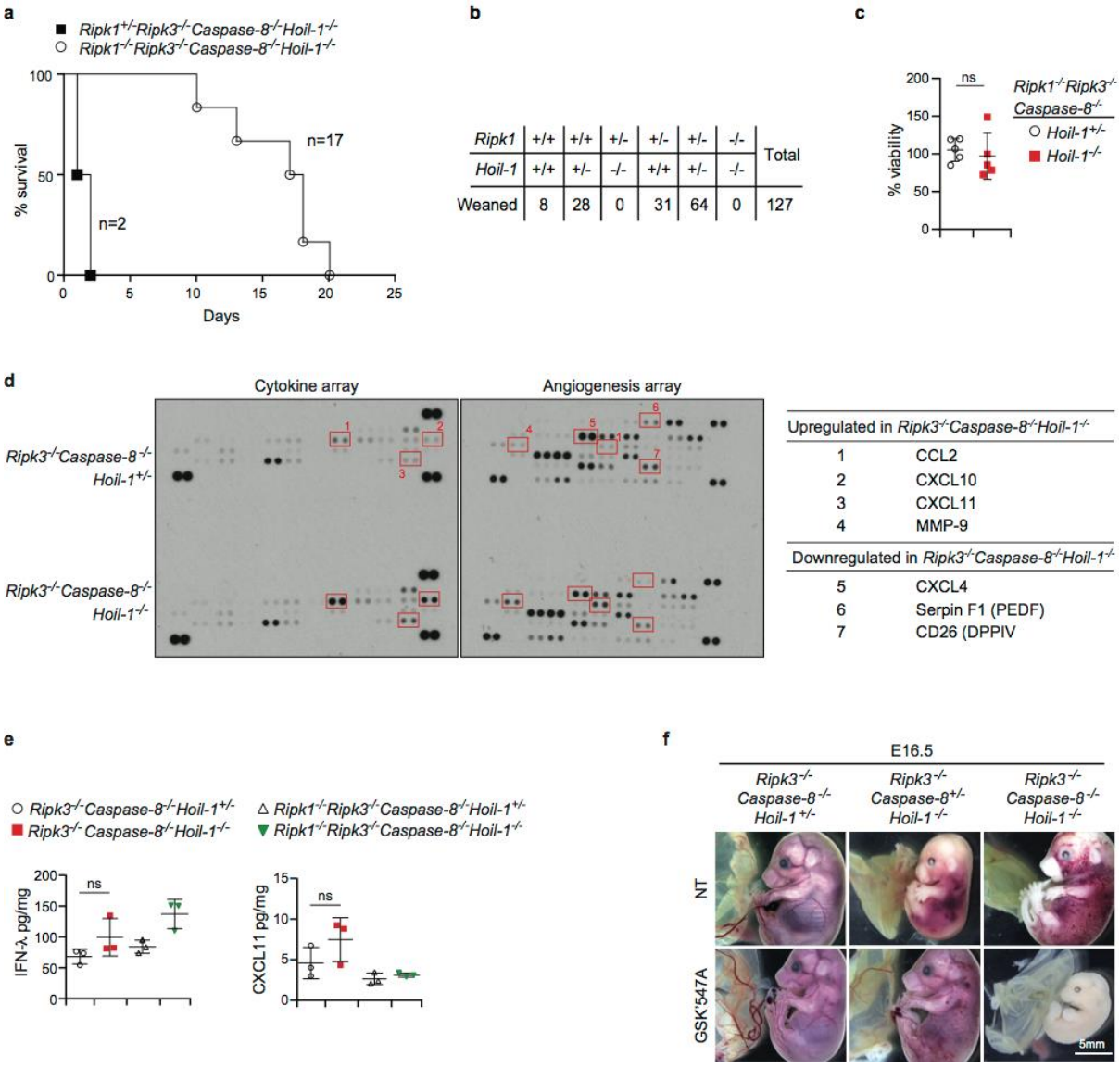

Extended Data Figure 10